Calcium carbonate dissolution triggered by high productivity during the last glacial-interglacial interval at the deep western South Atlantic

Jaime Y. Suárez-Ibarra[1], Cristiane Fraga Frozza[2], Sandro Monticelli Petró[3], Pamela Lara Palhano[2], and Maria Alejandra Gomez Pivel[2]

[1]Univerzita Karlova
[2]Universidade Federal do Rio Grande do Sul
[3]Universidade do Vale do Rio dos Sinos - UNISINOS

November 28, 2022

Posted on 28 Nov 2022 — CC-BY-NC 4 — https://doi.org/10.1002/essoar.10507115.1 — This a preprint and has not been peer reviewed. Data may be preliminary.

Abstract

Studies reconstructing surface paleoproductivity and benthic conditions allow us to measure the effectiveness of the biological pump, an important mechanism in the global climate system. In order to assess surface productivity changes and their effect on the seafloor, we studied the core SAT-048A, recovered from the continental slope of the southernmost Brazilian continental margin, in the western South Atlantic. We assessed the sea surface productivity, the organic matter flux to the seafloor and the dissolution effects, based on micropaleontological (benthic and planktonic foraminifers, ostracods), geochemical (benthic and planktonic δ13C isotopes) and sedimentological data (carbonate and bulk sand content). Superimposed on the climate-induced changes related to the last glacial-interglacial transition, the reconstruction indicates paleoproductivity changes synchronized with the precessional cycle. From the reconstructed data, it was possible to identify high (low) surface productivity, high (low) organic matter flux to the seafloor, and high (low) dissolution rates of planktonic Foraminifera tests during the glacial (postglacial). Furthermore, within the glacial, enhanced productivity was associated with higher insolation values, explained by increased NE summer winds that promoted meandering and upwelling of the nutrient-rich South Atlantic Central Water. Changes in the Atlantic Meridional Overturning Circulation and the reorganization of bottom water masses could also have changed the CO3 2- saturation levels and have influenced the carbonate preservation. However, changes in the Uvigerina spp. δ13C values are very likely linked to the organic matter flux and not to the sea bottom dissolved inorganic matter δ13C values.

Calcium carbonate dissolution triggered by high productivity during the last glacial-interglacial interval at the deep western South Atlantic

J.Y. SUÁREZ-IBARRA[1,2], C.F. FROZZA[1], S.M. PETRÓ[3], P.L. PALHANO[1], M.A.G. PIVEL[4]

[1]Programa de Pós-Graduação em Geociências, Instituto de Geociências, Universidade Federal do Rio Grande do Sul, Av. Bento Gonçalves, 9500, Cx. P. 15001, 91501-970, Porto Alegre, RS, Brazil.
[2]Ústav Geologie a Paleontologie, Přírodovědecká fakulta, Univerzita Karlova, Albertov 6, Praha 2, 12843, Czech Republic, present address.
[3]ITT FOSSIL - Instituto Tecnológico de Micropaleontologia, Universidade do Vale do Rio dos Sinos, Av. UNISINOS, 950, 93022-750, São Leopoldo, RS, Brazil.
[4]Instituto de Geociências, Universidade Federal do Rio Grande do Sul, Av. Bento Gonçalves, 9500, Cx. P. 15001, 91501-970, Porto Alegre, RS, Brazil.

Key Points:

- High summer insolation induced high glacial productivity in the study area.
- High surface productivity led to high organic matter flux to the seafloor.
- Seafloor dissolution was caused by surface conditions rather than water masses changes.

Corresponding author: J.Y. SUÁREZ-IBARRA, jysuarezibarra@gmail.com

Abstract

Studies reconstructing surface paleoproductivity and benthic conditions allow us to measure the effectiveness of the biological pump, an important mechanism in the global climate system. In order to assess surface productivity changes and their effect on the seafloor, we studied the core SAT-048A, recovered from the continental slope of the southernmost Brazilian continental margin, in the western South Atlantic. We assessed the sea surface productivity, the organic matter flux to the seafloor and the dissolution effects, based on micropaleontological (benthic and planktonic foraminifers, ostracods), geochemical (benthic and planktonic δ^{13}C isotopes) and sedimentological data (carbonate and bulk sand content). Superimposed on the climate-induced changes related to the last glacial-interglacial transition, the reconstruction indicates paleoproductivity changes synchronized with the precessional cycle. From the reconstructed data, it was possible to identify high (low) surface productivity, high (low) organic matter flux to the seafloor, and high (low) dissolution rates of planktonic Foraminifera tests during the glacial (postglacial. Furthermore, within the glacial, enhanced productivity was associated with higher insolation values, explained by increased NE summer winds that promoted meandering and upwelling of the nutrient-rich South Atlantic Central Water. Changes in the Atlantic Meridional Overturning Circulation and the reorganization of bottom water masses could also have changed the CO_3^{2-} saturation levels and have influenced the carbonate preservation. However, changes in the Uvigerina spp.δ^{13}C values are very likely linked to the organic matter flux and not to the sea bottom dissolved inorganic matter δ^{13}C values.

Keywords: Planktonic Foraminifera, Stable isotopes, Atlantic Meridional Overturning Circulation, Upper Circumpolar Deep Water, North Atlantic Deep Water.

1 Introduction

The Late Quaternary climate is characterized by orbit-related glacial-interglacial fluctuations (EPICA Community Members, 2004; Jouzel et al., 2007) associated to CO_2 variations (Petit et al., 1999; Shakun et al., 2012). Nevertheless, the orbital forcing *per se* is not strong enough to induce such temperature changes, and thus, feedbacks in the Earth's climate system are expected to amplify (or reduce) the primary signal (Lorius et al., 1990; Shackleton, 2000). An intensified biological pump in the oceans, and therefore an increase of exported biogenic carbon –along with biogenic carbonate– burial in the sediments (Brummer & van Eijden, 1992), is expected during glacial times as a mechanism to remove atmospheric CO_2. Since planktonic Foraminifera are important contributors of pelagic calcium carbonate flux (Milliman et al., 1999; Schiebel, 2002; Kučera, 2007) they represent an important piece in the global climate system, due to their capacity to remove CO_2 and contribute to its storage in the marine sediments.

However, high biological surface productivity can also: i) boost the benthic communities (Cronin et al., 1999), leading to the remineralization of higher percentages of organic matter (OM) and decreasing the biologic carbon burial; and ii) release more CO_2 (*e.g.,* due to respiration processes; Hales, 2003) and dissolve larger quantities of biogenic carbonate, (*e.g.,* planktonic Foraminifera tests; Schiebel, 2002). Therefore, the export of organic matter to the seabed can have a contrary effect (*e.g.,* Zamelczyk et al., 2012; Naik et al., 2014) regarding the biogenic carbonate burial.

The western South Atlantic is an ideal setting to study the effects of high OM fluxes to the seafloor given its well-documented high glacial productivity (Gu et al., 2017; Pereira et al., 2018; Portilho-Ramos et al., 2019). Therefore, this study reconstructs the past sea surface and bottom oceanographic conditions in this region, in terms of productivity, using a multiproxy analysis (micropaleontological, geochemical and sedimentological data), in order to improve the understanding of the benthic-pelagic dynamic during the last glacial-interglacial interval at the western South Atlantic.

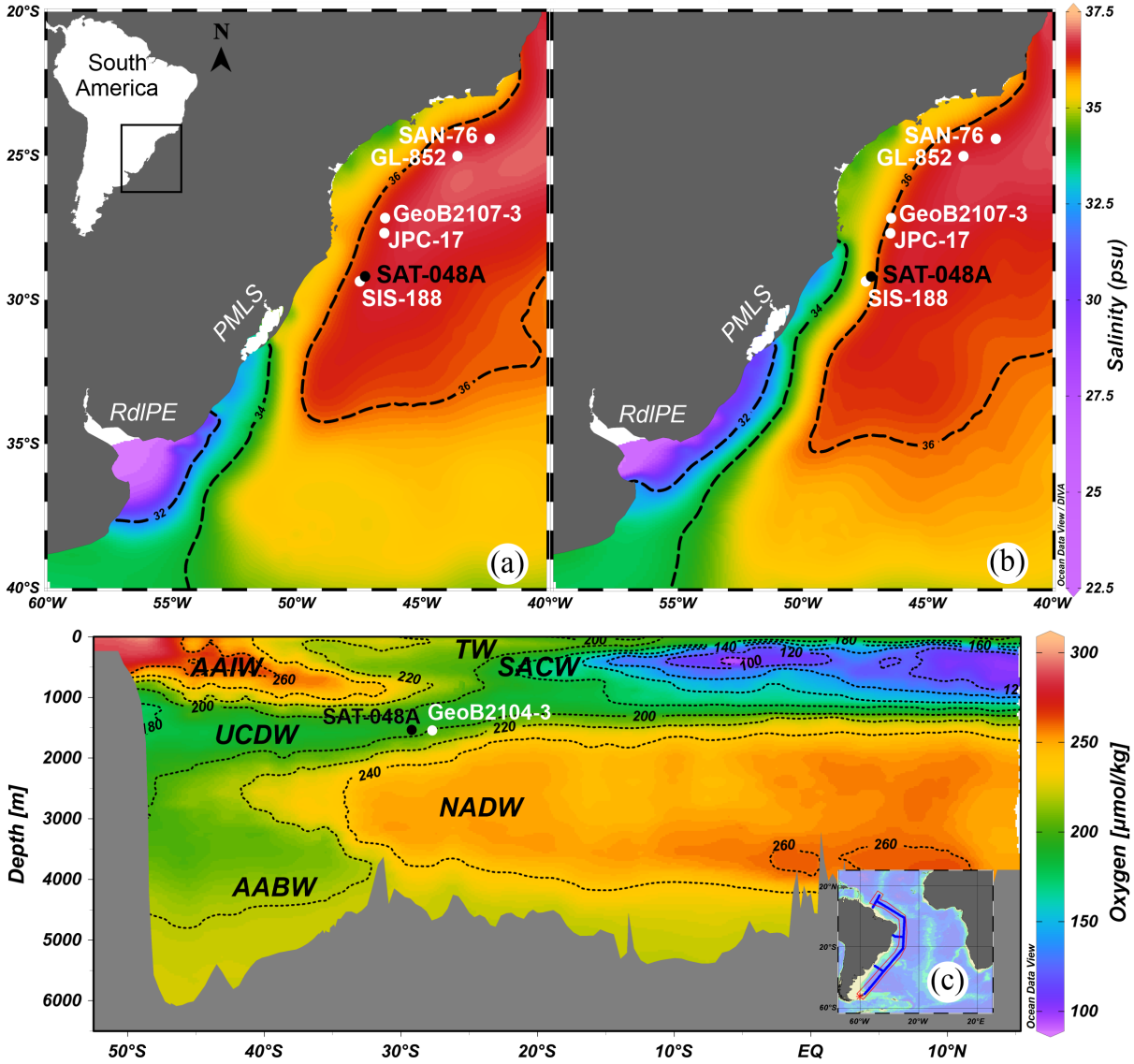


Figure 1. Location of core SAT-048A and other mentioned-cores (Supplementary material), plan view and latitudinal cross section. Seasonal variation of average sea surface salinity in the study area for the months of (a) January-March and (b) July-September, according to the World Ocean Atlas 2013 (WOA13, Zweng et al., 2013). The isohalines 32, 34 and 36 psu (dashed lines) highlight the less saline water intrusion from the south during the austral winter according to the wind regime. Present Río de la Plata Estuary (RdlPE) and Patos-Mirim Lagoon System (PMLS) represent important continental nutrient sources to the study area. The isolines (c) (dotted curves) of dissolved oxygen concentrations (μmol/kg) from a section of the South American continental margin showing the South Atlantic water masses that circulate in the region: Tropical Water (TW), South Atlantic Central Water (SACW), Antarctic Intermediate Water (AAIW), Upper Circumpolar Deep Water (UCDW), North Atlantic Deep Water (NADW) and Antarctic Bottom Water (AABW).

2 Regional setting

The studied core was recovered off Santa Marta Cape, at the Pelotas Basin slope, western South Atlantic (Figure 1a, b). The proximal portion of the continental shelf of the Pelotas Basin represents a submerged coastal plain (Martins, 1984) that was exposed during the last Pleistocene regression (Marine Isotope Stage 2) and dissected by drainage networks from fluvial systems (Weschenfelder et al., 2014), contributing with larger inputs of nutrients from continental outflows compared to the Holocene.

Surface circulation in the shelf portion of the study area is dominated by the northward Brazil Coastal Current, which carries the Coastal Water (CW), a mixture of oceanic and continental drainage waters. Offshore, the Brazil Current (BC) transports southward the warm (temperature, T>20°C) and salty (salinity, S>36 psu) Tropical Water (TW) at the surface layer. The BC flows along the South American margin slope until it converges with the Malvinas Current (MC), a northward surface current carrying cold (T<15°C) and fresher (S<34.2 psu) Subantarctic Water, forming the Brazil/Malvinas Confluence (BMC) close to 38°S (Gordon & Greengrove, 1986). The BMC forms a large meander which separates southward from the continental margin (Peterson & Stramma, 1991; Piola & Matano, 2017), and varies seasonally and interannually, moving to the north in austral autumn and winter, and to the south in spring and summer, influencing the nutrient distribution along the continental shelf of the Argentinian, Uruguayan and southern Brazilian coasts (Gonzalez-Silvera et al., 2006). Presently, two main continental sources of nutrients and freshwater for the area are the Río de la Plata Estuary (RdlPE) and the Patos-Mirim Lagoon System (PMLS). Although the configuration of continental drainage certainly changed under the varying sea-level conditions of the late Quaternary, they both represent sources of continental drainage, and thus, nutrients to the study area.

The water masses that circulate in the subsurface (Figure 1c) immediately below the TW are: South Atlantic Central Water (SACW), Antarctic Intermediate Water (AAIW), Upper Circumpolar Deep Water (UCDW), North Atlantic Deep Water (NADW) and Antarctic Bottom Water (AABW) (Reid et al., 1976; Campos et al., 1995; Hogg et al., 1996; Stramma & England, 1999). The NADW represents slightly warmer and saltier water bodies when compared to AAIW, UCDW and AABW. In addition, the NADW also promotes the preservation of carbonate, due to the oversaturation of the carbonate ion (CO_3^{2-}), in relation to the overlying UCDW and the underlying AABW, both undersaturated in CO_3^{2-} which, therefore, may lead to the dissolution of carbonate (Frenz et al., 2003). Indeed, the interface between the NADW and the AABW defines the depth of the lysocline (Frenz & Henrich, 2007), through which occurs a great change in the dissolution indexes.

3 Material and methods

The piston core SAT-048A was collected by *FUGRO Brasil – Serviços Submarinos e Levantamentos Ltda* for the *Agência Nacional do Petróleo* (ANP, Brazilian National Agency of Petroleum, Natural Gas and Biofuels) at 29°11'S, 47°15'W, 1542 m water depth (Figure 1). The core, with a total recovering of 315 cm, was sampled at intervals of about six cm, totalizing 54 samples. The core lacks the top 20 cm and the 196-217 cm interval (Figure 2). Each sample was washed over a 0.063 mm sieve and oven dried under temperatures below 60°C. The taxonomical identification of the planktonic Foraminifera species, from subsamples of at least 300 specimens larger than 0.15 mm, followed Bé (1967), Bé et al. (1977), Bolli & Saunders (1989), Hemleben et al. (1989), Kemle von Mücke & Hemleben (1999), Schiebel & Hemleben (2017) and Morard et al. (2019).

It was used a revised version of the Frozza et al. (2020) age model, carried out by Savian et al. (submitted), based on rbacon package (Blaauw & Christen, 2011; version

2.4.2) for the R software (R Core Team, 2019), considering the Laschamp geomagnetic excursion as a control point besides ten AMS radiocarbon dates.

Past Sea Surface Temperatures (SST) were estimated using the Modern Analogue Technique (MAT, Hutson, 1980) tool from the software PAST (version 3.2; Hammer et al., 2001), considering 100 meters below sea level (SST_{100m}). The paleo SST_{100m} were calibrated with a dataset composed as follows: i) relative abundances of planktonic Foraminifera of surface sediments from the South Atlantic Ocean extracted from the ForCenS database (Siccha & Kučera, 2017) coupled to ii) modern mean annual temperature estimates for 100 meters below sea level, obtained from the World Ocean Atlas 2013 (Locarnini et al., 2013), extracted with the software Ocean Data View (Schlitzer, 2020). For the Weighting parameter it was used the inverse dissimilarity, for the dissimilarity it was used the squared chord, a Threshold of 0.28 and five analogues.

Surface paleoproductivity was assessed from the relative abundances of the species *Globigerinita glutinata* (Conan et al., 2000; Souto et al., 2011) and the ratio between *Globigerina bulloides* and *Globigerinoides ruber (albus & ruber) (G.bull:G.rub*, Conan et al., 2002; Toledo et al., 2008). The OM flux to the seafloor was estimated based on the benthic:planktonic Foraminifera ratio (Berger & Diester-Haass, 1988; Loubere, 1991; Gooday, 2002), called B:P hereafter, the ostracods valves abundances (number of valves in the >150 μm fraction per gram of sediment), and the δ^{13}C record of *Uvigerina* spp. ($\delta^{13}C_{Uvi}$, Mackensen, 2008). Part of these data (*G. bulloides* %, *G. ruber* % and $\delta^{13}C_{Uvi}$) were previously published by Frozza et al. (2020). As a sea surface fertilization index, the δ^{13}C record of *G. ruber ruber* ($\delta^{13}C_{G.rub}$) was analyzed (Wefer et al., 1999). Approximately seven specimens of the benthic genus *Uvigerina* spp. and 12–15 specimens of the planktonic species *G. ruber ruber* were selected from the >250 μm fraction for each sample. The geochemical analyses were performed with a Thermo Scientific MAT-253 mass spectrometer, coupled to a Kiel IV carbonate device, by the Laboratory of Stable Isotopes of the University of California, Santa Cruz (SIL-UCSC). All results are expressed relative to the Vienna Pee-Dee Belemnite (VPDB) standard.

The dissolution effect was estimated based on the planktonic Foraminifera Fragmentation Intensity (Suárez-Ibarra et al., accepted manuscript), which follows Berger (1970)'s fragments and broken shells counting. Other dissolution effect indicators and proxies used were bulk sand fraction (%, Berger et al., 1982; Gonzales et al., 2017), the number of planktonic Foraminifera tests per gram (PF/g, Le & Shackleton, 1992) and $CaCO_3$ content (%). Bulk sand contents were determined using a laser diffraction particle size analyzer Horiba Partica-LA-950 at the Climate Studies Center (CECO, Centro de Estudos Climáticos) of the Universidade Federal do Rio Grande do Sul (UFRGS). The calcium carbonate content for the samples was determined by weight loss after reaction with 10% hydrochloric acid (HCl) at the Calcareous Microfossils Laboratory of the UFRGS. All dissolution data were previously published by Suárez-Ibarra et al. (accepted manuscript).

4 Results

The core SAT-048A sediments correspond to hemipelagic muds rich in carbonate. The average grain size of the samples is slightly sandy mud, ranging from slightly clayey mud to muddy sand in some cases. The recovered sediments correspond to the latest Pleistocene and early/middle Holocene muds of the Imbé Formation. The age model (Supplementary material) revealed a sediment recovery ranging from 43 to 5 ka BP, with sedimentation rates varying between 3 to 10 cm/kyr (Figure 2).

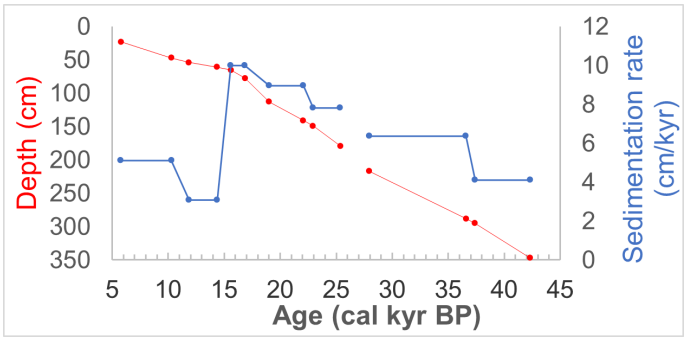


Figure 2. The sedimentation rate (cm/kyr) through the timespan recorded by core SAT-048A shows a progressive increase from 43 to 15 ka BP, when it decreases to a minimum between 14 and 11 ka BP and remains low until 5 ka BP. Data gap interval corresponds to unavailable samples.

4.1 Planktonic Foraminifera

Planktonic Foraminifera species display two contrasting temporal distribution patterns: i) species with higher abundance values during the Late Pleistocene that decreased towards the Holocene (*Globigerinita glutinata, Globigerina bulloides, Globoconella inflata* and *Neogloboquadrina incompta*; Figure 3a-d) and ii) species with lower abundance values during the Late Pleistocene and higher abundances in the Holocene (such as *Globigerinoides ruber albus* and *ruber, Trilobatus trilobus, Globorotalia menardii, Globigerinella calida, Orbulina universa, Globorotalia tumida* and *Globigerinoides conglobatus*; Figure 3e-l).

4.2 SST and Paleoproductivity estimates

Figure 4 presents the performance of the Modern Analogue Technique for the SST_{100m} reconstructions (Figure 4a), with an R^2 of 0.9932, and the annual mean past SST_{100m} estimates (Figure 4b) for core SAT-048A through time, while residuals are shown in the supplementary material. The annual mean SST_{100m} reconstructions showed lower values from the base until 37 ka BP (on average 16°C), although the lowest value occurred at 25 ka BP (15.2°C). More variable temperatures were obtained for the 37 – 15 ka BP period, ranging from 16 to 18°C. A warming trend was established from the Last Glacial Maximum (LGM) onwards, with values between 19 – 23°C and the warmest value (22.5°C) observed at 7 ka BP.

The paleoproductivity estimates are presented in Figure 5. For the 43 – 35 ka BP interval, the highest values were obtained for *G. glutinata* (Figure 5a), *G.bull:G.rub* ratio (Figure 5b) and B:P ratio (Figure 5c), followed by an interval (35 – 25 ka BP) characterized by lower values. Subsequently, from 25 to 13 ka BP, the *G. glutinata* and the B:P ratio exhibited relatively higher values at the end of this period, although generally smaller than those from the 43 – 35 ka BP interval. Meanwhile the *G.bull:G.rub* ratio showed higher values at the beginning of this period. From 13 ka BP onwards, a decreasing trend for the three tracers reaches the top (5 ka BP), registering the lowest values of the record. The geochemical tracers $\delta^{13}C_{G.rub}$ (Figure 5d) and $\delta^{13}C_{Uvi}$ (Figure 5e) showed similar fluctuations. The $\delta^{13}C_{G.rub}$ displayed low values for the 43 – 35 ka BP interval, followed by variable values until 19 ka BP. Finally, the lowest value (0.6‰) occurred at 16.8 ka BP, where an increasing trend was established. The $\delta^{13}C_{Uvi}$ showed the minimum values at the base of the core framed in an increasing trend during the 43 – 23 ka BP. Lower values were obtained during the 23 – 12 ka BP interval, followed by

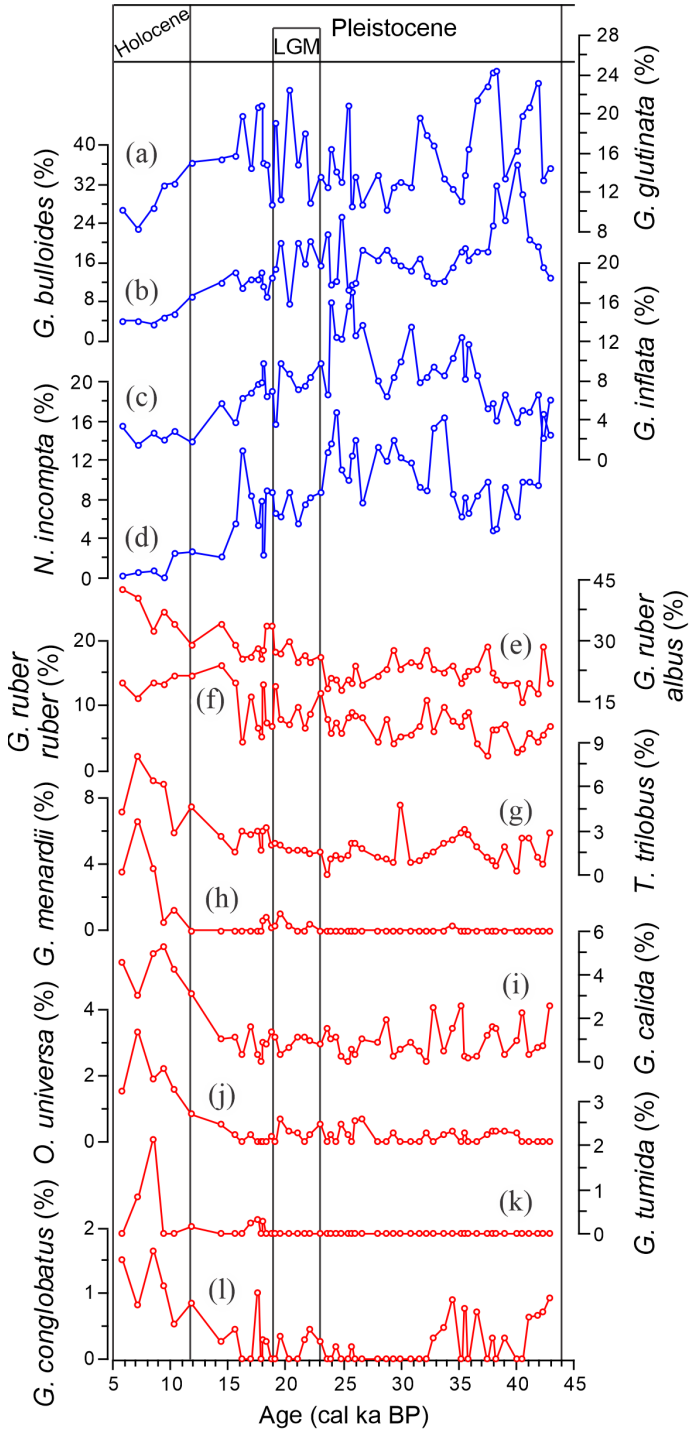


Figure 3. Relative abundances (%) of cool (blue, a-d) and warm (red, e-l) water species (Kučera, 2007) along the core SAT-048A from the recovered period. (a) *G. glutinata*, (b) *G. bulloides*, (c) *G. inflata*, (d) *N. incompta*, (e) *G. ruber albus*, (f) *G. ruber ruber*, (g) *T. trilobus*, (h) *G. menardii*, (i) *G. calida*, (j) *O. universa*, (k) *G. tumida* and (l) *G. conglobatus*. LGM: Last Glacial Maximum.

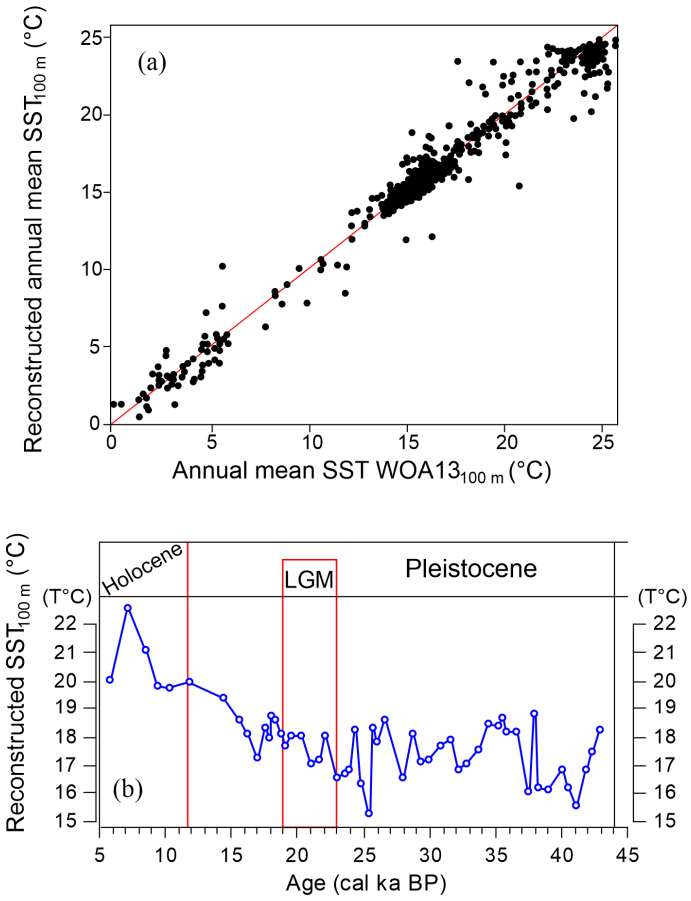


Figure 4. Modern Analogue Technique (MAT) performance and results of the annual mean paleotemperature estimates at 100 m waters below sea level (SST_{100m}) at the study site. (a) Regression ($R^2 = 0.9932$) curve between reconstructed annual mean SST_{100m} (°C) and the annual mean modern SST $WOA13_{100m}$ (°C) (Locarnini et al., 2013). (b) Reconstructed SST_{100m} (°C) along SAT-048A. LGM: Last Glacial Maximum.

increased values until the top. The ostracods' abundance (Figure 5f) showed low values during the 43 – 27 ka BP interval, when an increasing trend was established until 18 ka BP, followed by a decreasing trend until 5 ka BP.

4.3 Dissolution indicators

The Fragmentation Intensity (Figure 6a) showed a decreasing trend since 40 ka BP until 25 ka BP, with a plateau of relatively low values during the 36 – 32 ka BP interval. From 25 ka BP values increased until 17 ka BP, to then decrease until 11.8 ka BP, where the lowest value (0.31) was obtained. For the 11.8 – 5 ka BP interval, values increased again. In general terms, the $CaCO_3$ content (Figure 6b), the PF/g (Figure 6c) and Bulk sand content (Figure 6d) showed an increasing trend from 43 to 24 ka BP, although more variable for the Bulk sand content values. From 24 to 16 ka BP the trend was inverted, and values decreased. For the 16 – 12 ka BP period, a fast increase was registered, followed by decreasing values during the Holocene portion of the record.

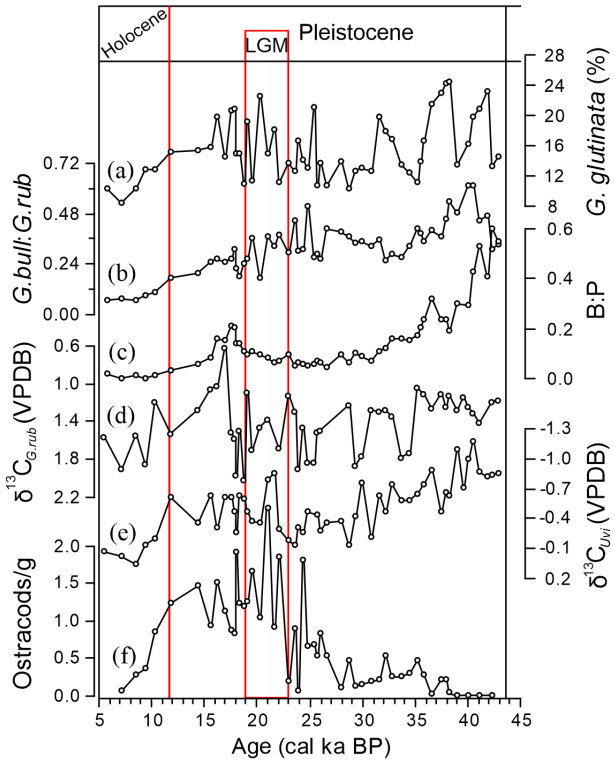


Figure 5. Paleoproductivity and paleofertility estimates for the core SAT-048A based on relative abundances (%) of (a) *G. glutinata*, (b) *G.bull:G.rub* ratio, (c) B:P (benthic:planktonic) Foraminifera ratio, (d) $\delta^{13}C_{G.rub}$, (e) $\delta^{13}C_{Uvi}$ and (f) ostracod abundance (number of valves/g). Inverted axes for (d) and (e) to aid visualization. LGM: Last Glacial Maximum.

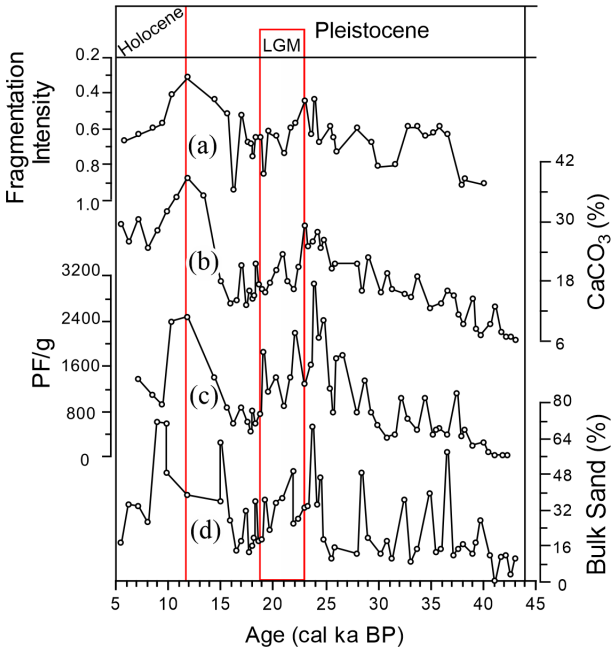


Figure 6. Dissolution indicators applied to the core SAT-048A: (a) Fragmentation Intensity, (b) $CaCO_3$ content (%), (c) PF/g (number of planktonic Foraminifera tests per gram of dry sediment) and (d) Bulk sand content (%). Inverted axes for (a) to aid visualization. LGM: Last Glacial Maximum.

5 Discussion

5.1 Long term fluctuations

Portilho-Ramos et al. (2019) explained the high productivity during the last glacial near the study area by two mechanisms: i) prolonged winter conditions and ii) short austral summer upwellings. The first implies prevalent southwesterly (SW) winds year-round carrying outflows from the Río de La Plata (RdlP) (Pimenta et al., 2005; Piola et al., 2005) and other continental sources (Camaquã, Jaguarão and Jacuí rivers) which presently converge in the PMLS, closer to the study area (Piola et al., 2000; Nagai et al., 2014). Strengthened SW winds would also displace the BMC closer to the area (Gonzalez-Silvera et al., 2006). The high relative abundance of *G. inflata* and *N. incompta* (Figure 3c, d) can be interpreted as a closer BMC (Boltovskoy et al., 1996), due to the enhanced SW winds during the late last glacial. The second mechanism involves the NE winds blowing along the shore, pushing surface waters offshore due to the Ekman transport, allowing summer upwelling (Chen et al., 2019).

Additionally, Mahiques et al. (2007) proposed that during low relative sea levels (glacial times) periods of higher nutrients and terrigenous sediments input were favored due to the more offshore position of the BC and the exposure of the continental shelf. Moreover, the Río de la Plata (Lantzsch et al., 2014) and Jacuí and Camaquã river paleodrainages (Weschenfelder et al., 2014) were closer to the study area during this interval (higher influence of the PMLS). Higher Fe/Ca values (Heil, 2006), higher proportion of eutrophic dinocysts (Gu et al., 2017) and high terrestrial palynomorphs proportions (Bottezini et al., 2019), are all evidence of the greater influence of continental outflow in the study area under lower relative sea levels of the late last glacial. In contrast, for the Holocene, the higher relative sea level and onshore displacement of the BC, as well as the absence of the SACW, inhibited the photic zone fertilization, leading to oligotrophic conditions (Mahiques et al., 2007).

The *G.bull:G.rub* ratio records from the western South Atlantic (Figure 7a-e) display a clear tendency to reduction since the LGM, except by a small increase in the Pleistocene/Holocene transition, also recorded in the cores SAN-76 (Toledo et al., 2007; Figure 7a) and JPC-17 (Portilho-Ramos et al., 2019; Figure 7c). A clear warming tendency starting at about 35 ka BP was registered by Lessa et al. (2019) (Figure 7g), with scarce data for the Pleistocene/Holocene transition. Warming trends during the LGM were also recorded by Portilho-Ramos et al. (2019) (Figure 7h) and more clearly by Pereira et al. (2018) (Figure 7i), although in the latter, cooler temperatures were reestablished prior to the LGM end. In the SAT-048A record (this study), SST_{100m} reconstructions showed variable cooler temperatures until 25 ka BP, and a warming and relatively stable trend afterwards, with the coolest temperatures being registered prior to the LGM (Figure 7j). Temperatures cooler than 20°C at 100 m water depth (Campos et al., 2000; Silveira et al., 2000; Castelão et al., 2004), along with *G.bull:G.rub* ratio values higher than 0.25 (Lessa et al., 2014), can be interpreted as a constant presence of the SACW in the subsurface during the short austral upwelling of the late glacial. The *G.bull:G.rub* ratios from the mentioned cores show no relation with the summer insolation (Figure 7), supporting Pereira et al. (2018) who stated no orbital cycle forcing.

The reported fluctuations took place in a context of gradual Atlantic Meridional Overturning Circulation (AMOC) weakening, leading to uninterrupted heat accumulation in the subtropical South Atlantic gyre and, therefore, a high glacial maxima out-of-phase (Santos et al., 2017). Luz et al. (2020) showed that this cool or warm water presence during the LGM is associated to the water masses that interplay at the surface near the continent: the offshore warm TW carried by the BC and the onshore cooler CW transported by the Brazil Coastal Current (BCC) (Luz et al., 2020, and references therein). The authors found that the alkenone-derived SST estimates varied according to the BC/BCC (TW/CW) influence: a shallower and closer to the coast core (RJ-1501) registered a late

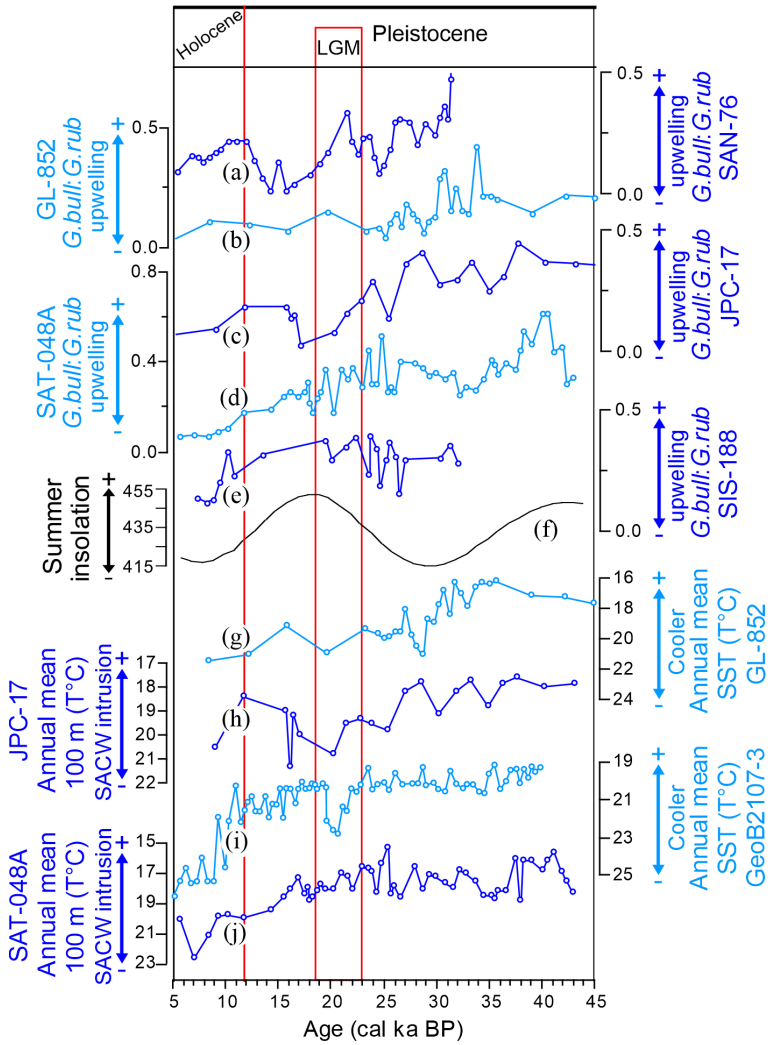


Figure 7. Higher *G.bull:G.rub* ratios and temperatures cooler than 20°C are interpreted as intrusions of the SACW in the subsurface, as a result of late glacial enhanced upwelling. *G.bull:G.rub* ratios of cores (a-e): (a) SAN-76 (Toledo et al., 2007), (b) GL-852 (Lessa et al., 2019), (c) JPC-17 (Portilho-Ramos et al., 2019), (d) SAT-048A (this study), (e) SIS-188 (Duque-Castaño et al., 2019), (f) austral summer (February) insolation at 31°S (Laskar et al., 2004); annual mean subsurface (100 m) temperatures for cores (g-j): (g) GL-852 (Lessa et al., 2019), (h) JPC-17 (Portilho-Ramos et al., 2019), (i) GeoB21073 (Pereira et al., 2018) and, (j) SAT-048A (this study).

deglacial warming, while in a deeper and more offshore core (RJ-1502), the early deglacial warming trend (Santos et al., 2017) was recognized.

5.2 Short term fluctuations

5.2.1 Surface paleoproductivity

Four intervals for the last 43 kyr can be defined according to the fluctuations in productivity indicators: IV (43 – 35 ka BP), III (35 – 24 ka BP), II (24 – 13 ka BP) and I (13 – 5 ka BP) (Figure 8). Intervals IV, III and II were characterized by higher productivity than interval I. But more interesting are the fluctuations during the late glacial, with intervals IV and II, characterized by a higher summer insolation (Figure 8a), which leads to stronger NE winds, strengthened BC, intensified meanderings and therefore, the enhancement of shelf break upwelling-fertilization (Portilho-Ramos et al., 2015; Pereira et al., 2018). This is inferred from: i) the increased relative abundance of *G. glutinata* (Conan et al., 2000; Souto et al., 2011) from cores GeoB2107-3 (Pereira et al., 2018; Figure 8b) and SAT-048A (this study; Figure 8c); ii) the higher relative abundance of *Globigerina falconensis* (Figure 8d) during intervals IV and II, associated with eutrophic conditions (Sousa et al., 2014), and iii) the relatively increased values of *Turborotalita quinqueloba* (Figure 8e), associated with intrusions of cooler SACW into the photic zone (Souto, et al., 2011; Lessa et al., 2014, 2016). Although quite variable from 35 – 18 ka BP, the $\delta^{13}C_{G.rub}$ (Figure 8g) increased values also corroborate the SACW intrusions (Venancio et al., 2014, 2016) and, therefore, higher fertilization in the area (Prell & Curry, 1981; Curry et al., 1992).

Additionally, the "silicic acid leakage hypothesis", brought by Portilho-Ramos et al. (2019) to explain high glacial productivity complements the "enhanced NE winds-enhanced SACW intrusions-enhanced subsurface productivity" dynamics. According to this hypothesis, glacial SACW enriched in dissolved $Si(OH)_4$ intruded the subsurface water during the short austral summer conditions, enhancing diatom blooms. Higher diatom record of Bottezini et al. (2019) and *G. glutinata* from SAT-048A and GeoB2107-3 (Pereira et al., 2018) for the late glacial support this hypothesis, since the species *G. glutinata*, that feeds on diatoms (Schiebel and Hemleben, 2017), can be favored under these conditions.

After high *G.bull:G.rub* ratio values and low SST_{100m} suggesting an enhanced upwelling of cool and nutrient-rich SACW intrusions for interval IV (Figure 9d), and a relatively not so productive interval III due to low summer insolation values and weaker NE winds (Figure 9c), it was expected an increase of *G.bull:G.rub* ratio and decrease of SST_{100m} during interval II, where higher upwelling would be expected because of the higher summer insolation and stronger NE winds (Figure 9b). The absence of an increasing trend can be associated to the record of heat accumulation in the South Atlantic subtropical Gyre (Santos et al., 2017; Luz et al., 2020), which was observed at about 25 ka BP for the SAT-048A core, coinciding with the beginning of interval II, and hampering upwelling. Another factor proposed as a fertilization control in the south Brazilian continental margin (SBCM) is the relative sea level variation (Gu et al., 2017; Pereira et al., 2018, Portilho-Ramos et al., 2019). Since during interval II (Figure 9b), the eustatic level was lower (Waelbroeck et al., 2002) than during interval IV (Figure 8o), a higher (terrigenous-related) fertilization was expected. However, paleoproductivity estimates for interval II are lower when compared to interval IV (Figure 8), suggesting a small role for the continental terrigenous fertilization for cores from mid-depths of the continental slope. Finally, during interval I (Figure 9a), NE winds were not strong enough to effectively pump SACW (which would also be depleted in silicic acid) to the photic zone (as shown by warmer SST_{100m}, low *G.bull:G.rub* ratio, and low relative abundance of *G. glutinata*). Furthermore, the onshore displacement of the BC, along with higher relative sea level, and rivers outflowing farther away, inhibited the terrigenous input, leading to oligotrophic conditions. Thus,

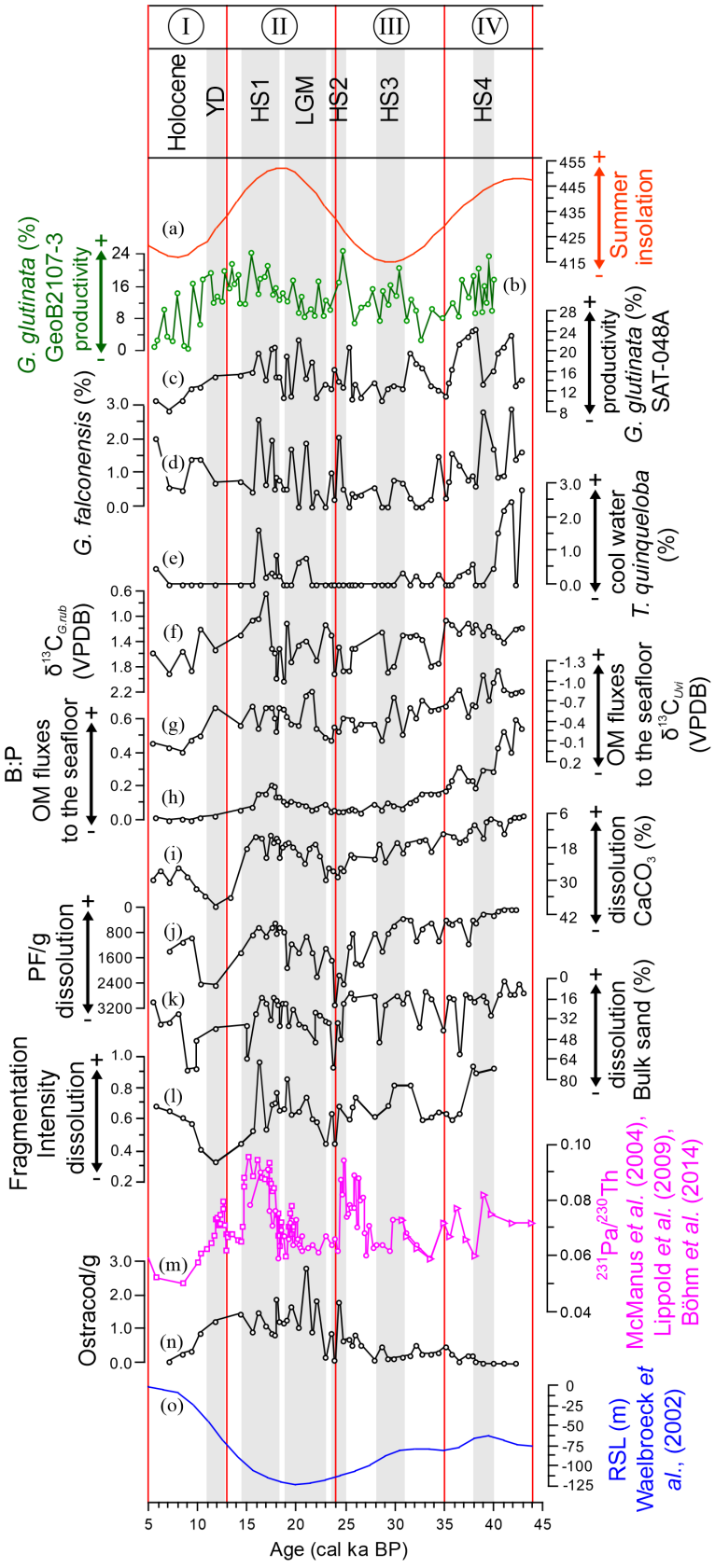


Figure 8. Caption on next page

Figure 8. Fluctuations in surface productivity, organic matter (OM) flux to the seafloor and planktonic foraminifers carbonate dissolution as a response to austral summer insolation variations at the study area. Intervals IV and II are characterized by very high productivity, III by high productivity and I by low productivity. (a) austral summer (February) insolation at 31°S (Laskar et al., 2004); relative abundances (%) of (b-e): (b) *G. glutinata* (GeoB2107-3, Pereira et al., 2018), (c) *G. glutinata* (SAT-048A), (d) *G. falconensis*, (e) *T. quinqueloba*; (f) $\delta^{13}C_{G.rub}$ (‰), (g) $\delta^{13}C_{Uvi}$ (‰), (h) B:P, benthic:planktonic Foraminifera ratio, (i) $CaCO_3$ content (%), (j) PF/g (number of planktonic Foraminifera tests per gram), (k) Bulk sand content (%), (l) Fragmentation Intensity, (m) $^{231}Pa/^{230}Th$ values from McManus et al. (2004, squares), Lippold et al. (2009, circles) and Böhm et al. (2014, triangles), (n) Ostracods per gram (valves/g), and (o) RSL (m, Relative Sea Level, Waelbroeck et al., 2002). Inverted axes in (f), (g) and (i-k) to aid visualization. Proxies in black belong to core SAT-048A.

based on the aforementioned data, it is possible to infer that the orbital forcing was able to modulate the productivity fluctuations in the study area, for the last glacial-interglacial transition, supporting previous studies from the western South Atlantic (*G. bulloides* – Lessa et al., 2017, 2019; eutrophic environmental dinocysts – Gu et al., 2017; Portilho-Ramos et al., 2019) and the North Atlantic (*e.g.,* Villanueva et al., 1998).

5.2.2 Organic matter flux to the seafloor

Orbital to suborbital climate cycles can influence the abundance shifts of deep-sea benthic communities (Cronin et al., 1999). Since abundance fluctuations of benthic Foraminifera and ostracods are related to variations in particulate organic carbon fluxes to the seafloor (Smith et al., 1997; Rex et al., 2006; Rex & Etter, 2010), their use as surface paleoproductivity indicators is widespread (Nees et al., 1999; Herguera, 2000; Rasmussen et al., 2002; Gooday, 2003; Yasuhara et al., 2012). The surface productivity fluctuations, indicated by *G. glutinata* (Figure 8c), are similar to those of the OM flux recorded by the B:P ratio (Figure 8h). This effective OM exportation (from the surface to the seafloor) revealed a high benthic-pelagic coupling (Toledo et al., 2007). Intervals II and IV show higher OM flux than I and III, with lower contributions registered during the Holocene, when oligotrophic conditions prevail. The B:P changes are inversely accompanied by similar $\delta^{13}C_{Uvi}$ trends (Figure 8g), which are expected to decrease when higher OM fluxes, rich in ^{12}C due to the preferential incorporation of the light isotope during photosynthesis (Wefer et al., 1999), reach the seabed (Ravello & Hillaire-Marcel, 2007). The B:P ratio showed a positive linear relationship with productivity, whereas ostracods valves abundance showed a hump-shaped relation with productivity (Yasuhara et al., 2012), increasing under enhanced – but still moderate – supply of OM and declining under very high productive conditions, where oxygen levels tend to decrease, and deep-sea ostracods, mostly epifaunal (Jöst et al., 2017), would not respond well to this environment. Additionally, abundance oscillations of deep-sea benthic organisms can also be related to paleobathymetric variations, decreasing exponentially with depth increase (Rex et al., 2006; Rex & Etter, 2010). However, a 120 m range in relative sea level changes during the late Quaternary is not sufficient to explain the observed abundance changes at mid-depths of the continental slope. While the ostracods record showed a negative relation (Figure 8n), the B:P ratio did not follow the same fluctuations than the relative sea level (Figure 8o).

Dissolution indicators showed higher calcium carbonate dissolution during intervals IV and II (Figure 8i-l), and their fluctuations are related to the OM flux. Enhanced dissolution could be triggered by two different processes: i) fluctuations in CO_2 concen-

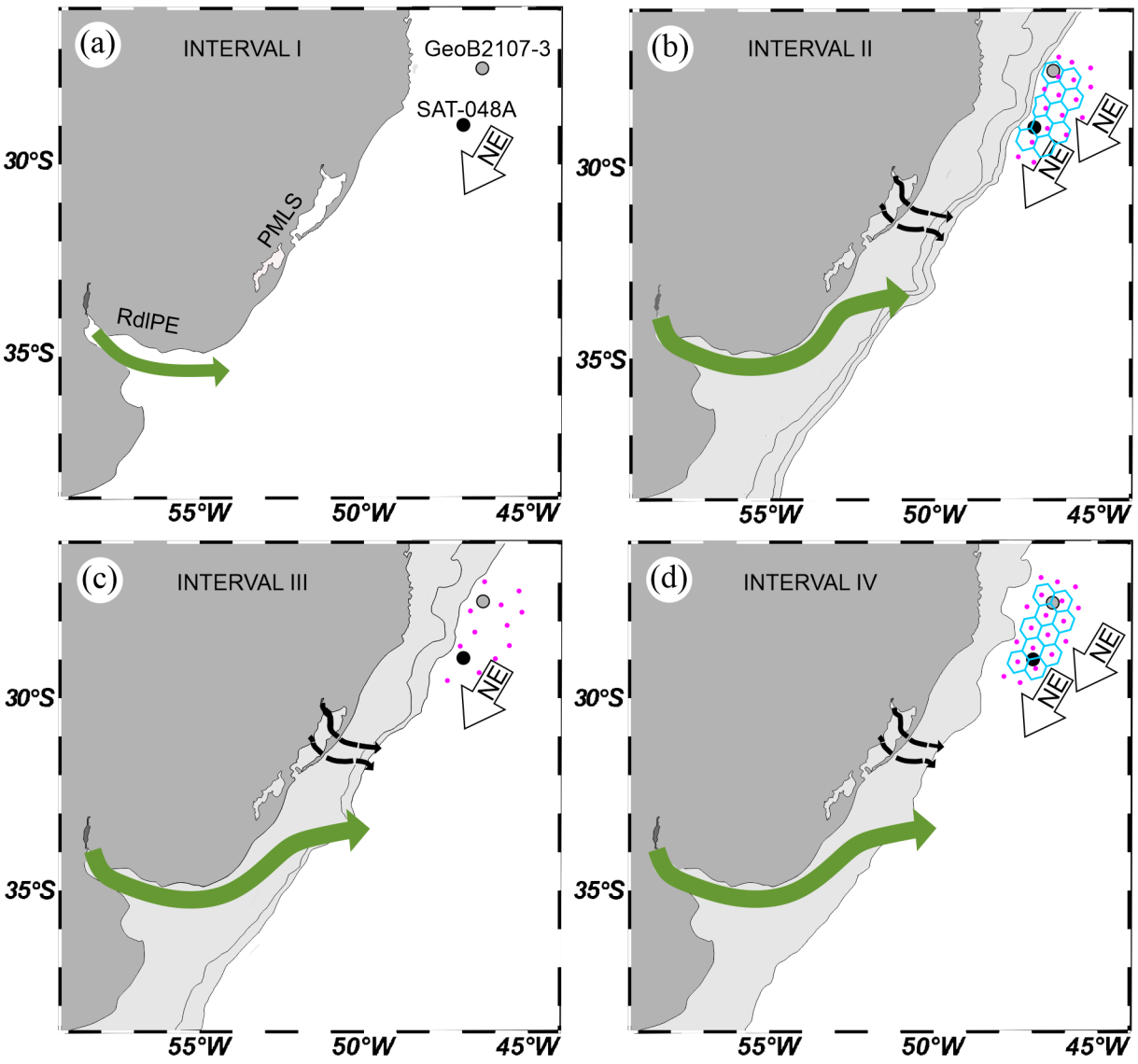


Figure 9. Schematic sea surface reconstruction for the study area next to the cores SAT-048A (this study) and GeoB2107-3 (Pereira et al., 2018). In light gray, (paleo)relative sea levels according to Waelbroeck et al. (2002) for the time interval, which in turn represent the exposed continental shelf. During interval I (a), the terrigenous nutrients input into the coastal surface waters by RdlPE (Río de la Plata Estuary, green arrows, Lantzsch et al., 2014), Jacuí and Camaquã paleo-rivers (nowadays Patos-Mirim Lagoon System, PMLS; black arrows, Weschenfelder et al., 2014) discharges is further away than during intervals II (b), III (c) and IV (d). In intervals IV and II, enhanced northeast (NE) winds triggered subsurface water pumping (blue honeycomb), as a mechanism of subsurface water fertilization. Pink dots represent intrusions in subsurface water rich in dissolved $Si(OH)_4$ (Portilho-Ramos et al., 2019), which were enhanced during the strengthened NE winds (intervals IV and II). Intervals: I (13 – 5 ka BP), II (24 – 13 ka BP), III (35 – 24 ka BP) and IV (43 – 35 ka BP).

trations (decreasing pH) due to the remineralization of OM at the seafloor (Jahnke et al., 1997; Schiebel, 2002) (Figure 10) or ii) the reorganization of bottom water masses related to AMOC dynamics. Although the B:P ratios are also used as a dissolution indicator (Berger & Diester-Haass, 1988; Conan, 2002), Kučera (2007) states it is only applied for abyssal depths.

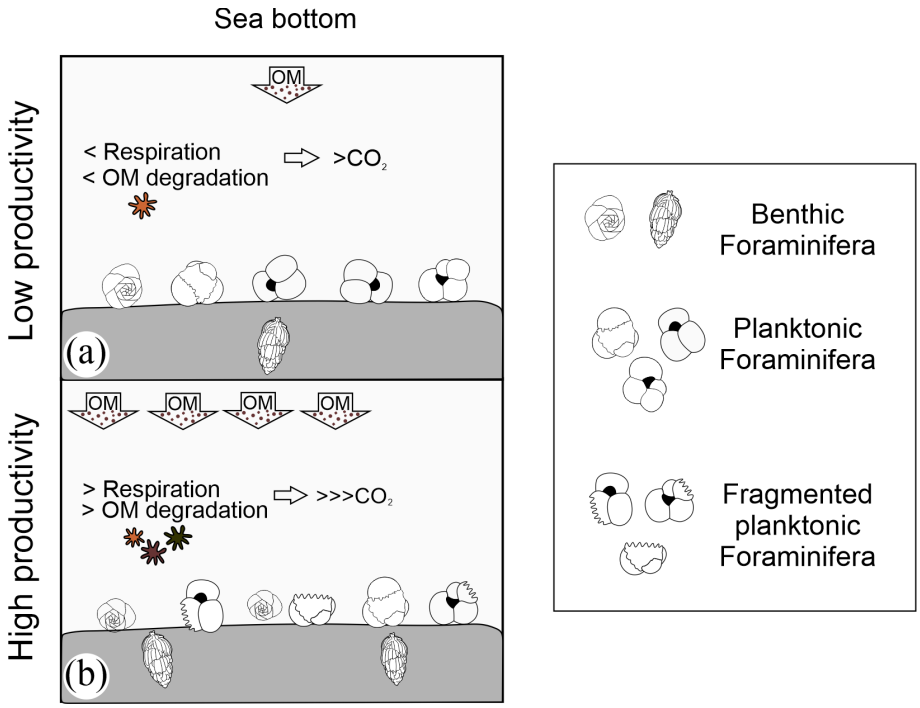


Figure 10. Schematic representation of the two possible settings affecting dissolution on deep-water assemblages of core SAT-048A. The paleoceanographic changes could be triggered by: (a) low OM inputs at the sea floor which results in lower benthic abundances and better preservation of $CaCO_3$, and (b) high OM inputs that increase benthic abundances, rise CO_2 concentrations, decrease the pH of the water and dissolve the planktonic Foraminifera tests (fragmentation on benthic Foraminifera was not assessed).

In the SBCM basins, the $\delta^{13}C_{Uvi}$ values have been used to infer oscillations of OM inputs (Toledo et al., 2007; Rodrigues et al., 2018; Dias et al., 2018; Frozza et al., 2020). Nevertheless, $\delta^{13}C_{Uvi}$ values involve several controlling factors, such as accumulation rates of organic carbon, regional changes of water masses, global carbon cycle, photosynthesis-respiration processes, temperature, and pH (Zahn, 1986; Ravelo & Hillaire-Marcel, 2007; Hesse et al., 2014). Lund et al. (2015) suggested that lower values of benthic $\delta^{13}C$ during glacial times are associated to a weak AMOC, which lead to: i) a pre-deglacial BC warming trend and the accumulation of heat in the South Atlantic subtropical gyre (Santos et al., 2017), due to a reduced exportation of heat and salt to the North Atlantic through the North Brazil Current, ii) the shallowing of the NADW due to lower density values, being restricted to the upper 2.5 km during the LGM and iii) the reconfiguration of the water masses (Curry & Oppo, 2005; Lynch-Stieglitz et al., 2006). However, according to Lund et al. (2015)'s logic, the $\delta^{13}C_{Uvi}$ more negative values during interval II would suggest the higher presence of the UCDW, (Figure 11) what contrasts with the shoaling of NADW during the LGM, and therefore, changes in $\delta^{13}C_{Uvi}$ probably do not mainly reflect the water $\delta^{13}C$ variations but other factors.

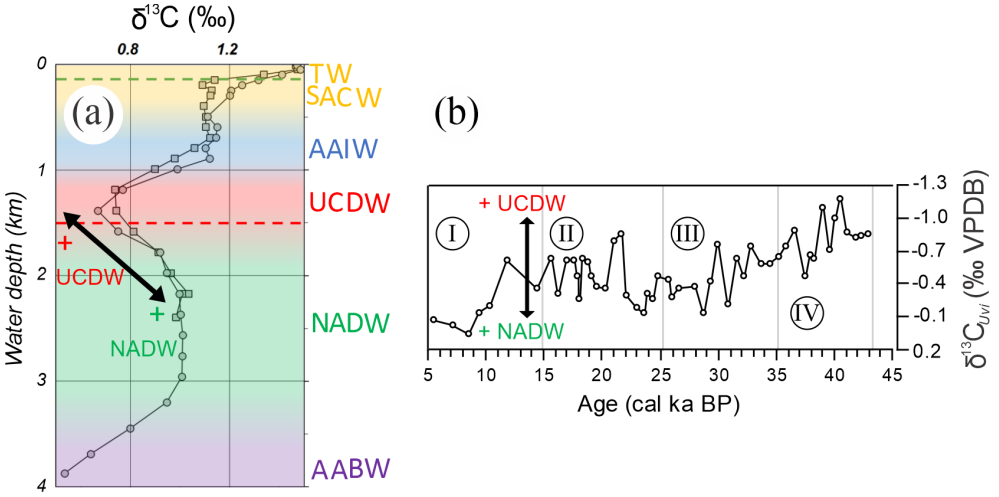


Figure 11. Modern isotopic signature of the different water masses present and the study area for the study site and values from the benthic genus *Uvigerina* from core SAT-048A. On (a) profile for the study area of the δ^{13}C variations according to depth (GLODAPv2, Olsen et al., 2016, 2019) and (b) $\delta^{13}C_{Uvi}$ results along the core SAT-048A. From (a) it could be possible to infer on (b) a higher NADW influence when $\delta^{13}C_{Uvi}$ values are more positive, which meant that $CaCO_3$ was better preserved than during the UCDW presence (Frenz et al., 2003). Gray vertical lines in (b) divides intervals IV-I. TW: Tropical Water, SACW: South Atlantic Central Water, AAIW: Antarctic Intermediate Water, UCDW: Upper Circumpolar Deep Water, NADW: North Atlantic Deep Water, and AABW: Antarctic Bottom Water.

The carbonate preservation and the fluctuations of $\delta^{13}C_{Uvi}$ could be the result of the interplay between the OM flux and water masses changes. However, the fluctuation range of $\delta^{13}C_{Uvi}$ values (Figure 11b) is up to 1‰, i.e. two times higher than the difference between the present-day δ^{13}C of dissolved inorganic carbon values for the UCDW and the NADW which is up to up to 0.4‰ (Fig 11a). Therefore, the observed pattern is more likely linked to changing OM fluxes to the seafloor. Aditionally, after δ^{13}C "corrections" (e.g., Schmiedl et al., 2004; -2‰) from benthic foraminifers tests and ambient bottom water, SAT-048A $\delta^{13}C_{Uvi}$ still remains more negative from the supposed original values, which also points to the input of OM fluxes, richer in ^{12}C than ^{13}C.

Based on ϵNd in benthic Foraminifera at mid-depths at the western South Atlantic, Howe et al. (2016b, 2018) showed variations of water masses inter-phase depths at 1000-1200 m (GeoB2107-3 and KNR159-3-36GGC) and 2200 m (GL-1090). After the Heinrich Stadial 1, core GL-1090 ϵNd values decreased, becoming more related to modern upper NADW values, while cores GeoB2107-3 and KNR159-3-36GGC ϵNd values increased after about 10 ka BP, showing more affinity with modern AAIW. But between the aforementioned cores is located core GeoB2104-3 (1500 m) – at the same depth of the here studied core SAT-048A–, which ϵNd values remained stable during 25 - 4 ka BP (Howe et al., 2016b). This i) suggests that if recent water masses distribution has kept stable since 4 ka BP, based on ϵNd in benthic Foraminifera of core GeoB2104-3, the SAT-048A $\delta^{13}C_{Uvi}$ points to the presence of the NADW, contradicting direct measures which would indicate the presence of the UCDW (Figure 1C, Figure 11A); and ii) indicates that SAT-048A $\delta^{13}C_{Uvi}$ fluctuations were actually produced by the OM bottom flux rather than water masses reconfiguration, since there were no changes through the register. This idea is supported by Howe et al. (2016a), where the authors stated that depleted glacial δ^{13}C

values in the deep Atlantic are not solely explained by water masses changes but also by high respired carbon accumulated on a sluggish deep overturning cell.

In addition, the $^{231}Pa/^{230}Th$ ratio, used to track the intensity of the AMOC (McManus et al., 2004; Lippold et al., 2009; Böhm et al., 2014) – where lower values mean a strengthened AMOC – can also shed a light on the discussion. In periods of high $^{231}Pa/^{230}Th$ values and AMOC slowdown (like Heinrich Stadials), a higher concentration of respired CO_2 is accumulated at seafloor water masses, as proposed by Howe et al. (2016a), being a possible explanation for the higher calcium carbonate dissolution intervals. But when compared, the $^{231}Pa/^{230}Th$ values (Figure 8m) and the dissolution proxies (Figure 8i-l), no relation is found during interval IV, where high dissolution contrasts with the intermediate $^{231}Pa/^{230}Th$ ratios. Also, during interval III and the transition to interval II, high $^{231}Pa/^{230}Th$ values did not cause high dissolution. Only a good match can be observed at the Heinrich Stadial 1, where both, high productivity and high dissolution, coincide with an interval of sluggish AMOC, as suggested by the high $^{231}Pa/^{230}Th$ ratios.

Finally, since the AMOC's intensity do not to explain the whole changes in the calcium carbonate dissolution in core SAT-048A, the surface productivity and OM flux to the seafloor is shown as the principal agent of the calcium carbonate dissolution, related to orbital forcings. Furthermore, special attention must be taken when interpreting Fe/Ca ratios, since higher values can be the response of i) higher Fe input but also to ii) high productivity and high OM fluxes to the sea floor that lead to calcium carbonate dissolution – as here explained –, contrary to the stated by Pereira et al., (2018), where the authors, when interpreting the ln(Fe/Ca) ratios from Heil (2006), affirmed that higher ln(Fe/Ca) values can not be result of high productivity due to the expected higher input of carbonatic tests to the sea floor, disregarding the effects of high OM fluxes. Further studies must explore the impact of the biological pump in the benthic $\delta^{13}C$ values of the deep South Atlantic to quantify their relation, as well as the Total Organic Carbon burial to better understand the glacial inorganic carbon sequestration hypothesis.

6 Conclusions

Planktonic Foraminifera assemblages from core SAT-048A, along with geochemical analyses and sedimentological data, enabled us to reconstruct the surface and bottom paleoceanographic fluctuations that occurred – in phase – during the last 43 kyr at the western South Atlantic, and to contextualize the related processes in the area. In long term changes, the Pleistocene-Holocene transition witnessed a shift from glacial eutrophic environment to more oligotrophic post-glacial conditions, as suggested by the *G.bull:G.rub* ratio and the SST_{100m}, where intrusions of the nutrient-rich SACW were inhibited and the Río de la Plata Estuary (RdlPE) and local river discharges (nowadays PMLS) were placed further away from the core site. In short term changes, the orbital-scale fluctuations of the upwelling dynamics (indicated by *G. glutinata*, *T. quinqueloba* and $\delta^{13}C_{G.rub}$), modulated by insolation and NE wind changes, influenced directly the surface productivity and the OM fluxes to the seafloor (as shown by the B:P ratio and $\delta^{13}C_{Uvi}$). Imposed to the already well-known mechanisms behind the high glacial productivity, the stronger NE winds, strengthened BC and increasing meanders – generated by precessionally-controlled higher insolation – enhanced the intrusion of cooler and nutrient-richer waters in subsurface for 43 – 35 and 24 – 13 ka BP, fertilizing the photic zone. The enhanced upwelling conditions were also registered at the sea floor, where the bacterial decomposition of OM and the respiration of higher abundances of benthic communities increased the CO_2 concentration, creating more acidic conditions that caused different levels of carbonate dissolution. Nevertheless, the reorganization of deep waters could cause the alternation of two water masses in contact with the core location seabed: i) the NADW, linked to preservation of $CaCO_3$ and, ii) the UCDW, related to $CaCO_3$ dissolution, due to its CO_3^{2-} undersaturated condition. Even though the registrated fluctuations of $\delta^{13}C_{Uvi}$

values are two times bigger than the difference between modern UCDW and NADW $\delta^{13}C$ values of the dissolved inorganic carbon (1‰ *vs.* 0.4‰), along with its more negative values and the geometric (ϵNd in benthic Foraminifera) and intensity ($^{231}Pa/^{230}Th$) proxies of water masses, point to the control of the OM fluxes. Additionally, the continental influence (*i.e.,* terrigenous input) must be better assessed, since no increased productivity was registered during the lowest relative sea level (LGM). Finally, the dissolution of planktonic Foraminifera tests, induced by an enhanced biological pump (evidenced in the high glacial surface productivity and the high OM fluxes to the sea floor), must call the attention to future research since our study area is not effective for removing, sinking and stocking glacial biogenic carbonates.

Acknowledgments

This work was supported by the Brazilian Coordination of Higher Education Staff Improvement (CAPES) (grant number 88887.091729/2014-01) and the Brazilian National Council for Scientific and Technological Development (CNPq) (grant number 407922/2016-4). The authors are grateful to Prof. Gilberto Griep (in memoriam) for his commitment to making sediment cores retrieved for the industry available to the scientific community. We are also grateful to Maria Helena Saraiva and Tiago Menezes Freire for sample processing and to Igor Venâncio, João Coimbra and Geise dos Anjos Zerfass for comments and suggestions. J.Y.S.I. thanks the CNPq for his master's scholarship. C.F.F. thanks CAPES for her PhD scholarship. The data presented in this paper is under submission process on the virtual repository Pangaea.

References

Bé, A.W.H. (1967). *Foraminifera Families: Globigerinidae and Globorotaliidae*, CONSEIL PERMANENT INTERNATIONAL POUR L'EXPLORATION DE LA MER, Zooplankton, 108, (1–9). Charlottenlund, Denmark: Conseil International pour l'Exploration de la Mer.

Bé, A.W.H., Hemleben, C., Anderson, O.R., Spindler, M., Hacunda, J., & Tuntivate-Choy, S. (1977). Laboratory and Field Observations of Living Planktonic Foraminifera. *Micropaleontology*, 23(2), 155–179.

Berger, W.H. (1970). Planktic Foraminifera: selective solution and the lysocline. *Marine Geology*, 8, 111–138.

Berger, W.H., Bonneau, M.-C., & Parker, F.L. (1982). Foraminifera on the deep-sea floor: lysocline and dissolution rate. *Oceanologica acta*, 5(2), 249–258.

Berger, W.H., & Diester-Haass, L. (1988). Paleoproductivity: the benthic/planktonic ratio in Foraminifera as a productivity index. *Marine Geology*, 81, 15–25. https://doi.org/10.1016/0025-3227(88)90014-X

Blaauw, M., & Christen, J.A. (2011). Flexible Paleoclimate Age-Depth Models using autoregressive gamma process. *Bayesian Analysis*, 6(3), 457–474. https://doi.org/10.1214/11-BA618

Böhm, E., Lippold, J., Gutjahr, M., Frank, M., Blaser, P., Antz, B., Fohlmeister, J., Frank, N., Andersen, M.B., & Deininger, M. (2015). Strong and deep Atlantic meridional overturning circulation during the last glacial cycle. *Nature*, 517, 73-76. https://doi.org/10.1038/nature14059

Bolli, H.M., & Saunders, J.B. (1985). *Oligocene to Holocene low latitude planktic foraminifera*, in: Plankton Stratigraphy, Bolli, H.M., Saunders, J.B., Perch-Nielsen, K. Cambridge Earth Sciences Series. Cambridge University Press, 1, 155–262.

Boltovskoy, E., Boltovskoy, D., Correa, N., & Brandini, F. (1996). Planktic foraminifera from the southwestern Atlantic (30°–60°S): species-specific patterns in the upper 50 m. *Marine Micropaleontology*, 28, 53–72. https://doi.org/10.1016/0377-8398(95)00076-3

Bottezini, S.R., Leonhardt, A., Diniz, D., & Gonçalves, J.F. (2019). Influência da drenagem continental sobre a paleoprodutividade na Bacia de Pelotas com base em palinomorfos: uma análise preliminar. *II Simpósio Brasileiro de Geologia e Geofísica Marinha*.

Brummer, G.J.A., & van Eijden, A.J.M. (1992). "Blue-ocean" paleoproductivity estimates from pelagic carbonate mass accumulation rates. *Marine Micropaleontology*, 19, 99–117. https://doi.org/10.1016/0377-8398(92)90023-D

Campos, E.J.D., Gonçalves, J.E., & Ikeda, Y. (1995). Water mass characteristics and geostrophic circulation in the South Brazil Bight: Summer of 1991. Journal of geophysical research, 100(9), 18537–18550.

Campos, E.J.D., Velhote, D., & Silveira, I.C.A. (2000). Shelf break upwelling driven by Brazil Current Cyclonic meanders. *Geophysical research letters*, 27, 751–754. https://doi.org/10.1029/1999GL010502

Castelão, R.M., Campos, E.J.D., & Miller, J.L. (2004). A Modelling Study of Coastal Upwelling Driven by Wind and Meanders of the Brazil Current. *Journal of Coastal Research*, 20(3(203)), 662–671. https://doi.org/10.2112/1551-5036(2004)20[662:AMSOCU]2.0.CO;2

Chen, H.H., Qi, Y., Wang. Y., & Chai, F. (2019). Seasonal variability of SST fronts and winds on the southeastern continental shelf of Brazil. *Ocean Dynamics*, 69, 1387–1399. https://doi.org/10.1007/s10236-019-01310-1

Conan, S.M.-H., & Brummer, G.J.A. (2000). Fluxes of planktic foraminifera in response tomonsoonal upwelling on the Somalia Basin margin. *Deep Sea Research Part II: Topical Studies in Oceanography*, 47(9–11), 2207–2227. https://doi.org/10.1016/s0967-0645(00)00022-9

Conan, S.M.-H., Ivanova, E., & Brummer, G.-J. (2002). Quantifying carbonate dissolution and calibration of foraminiferal dissolution indices in the Somali Basin. *Marine Geology*, 182(3-4), 325–349. https://doi.org/10.1016/s0025-3227(01)00238-9

Cronin, T.M., De Martino, D.M., Dwyer, G.S., & Rodriguez-Lazaro, J. (1999). Deep-sea ostracode species diversity: response to late Quaternary climate change. *Marine Micropaleontology*, 37(3–4), 231–249. https://doi.org/10.1016/S0377-8398(99)00026-2

Curry, W.B., Osterman, D.R., Guptha, M.V.S., & Ittekkot, V. (1992). *Foraminiferal production and monsoonal upwelling in the Arabian Sea: Evidence from sediment traps*; In: Upwelling Systems; Evolution Since the Early Miocene (eds) Summerhays, C.P., Prell, W.L. Emeis, K.C., Geol. Soc. of London, England, pp. 93–106.

Curry, W.B., & Oppo, D.W. (2005). Glacial water mass geometry and the distribution of δ^{13}C of $\sum CO_2$ in the western Atlantic Ocean. *Paleoceanography*, 20, PA1017. https://doi:10.1029/2004PA001021

Dias, B.B., Barbosa, C.F., Faria, G.R., Seoane, J.C.S., & Albuquerque, A.L.S. (2018). The effects of multidecadal-scale phytodetritus disturbances on the benthic foraminiferal community of a Western Boundary Upwelling System, Brazil. *Marine Micropaleontology*, 139, 102–122. https://doi.org/10.1016/j.marmicro.2017.12.003

Duque-Castaño, M.L., Leonhardt, A., & Pivel, M.A.G. (2019). Morphometric analysis in the shells of the planktonic Foraminifera Orbulina universa: a source for paleoceanographic information?. *Brazilian Journal of Oceanography*. 67, 1–17. https://doi.org/10.1590/S1679-87592019025206701

EPICA Community Members. (2004). Eight glacial cycles from an Antarctic ice core. *Nature*, 429, 623–628. https://doi.org/10.1038/nature02599

Frenz, M., Höppner, R., Stuut, J.-B.W., Wagner, T., & Henrich, R. (2003). *Surface Sediment Bulk Geochemistry and Grain-Size Composition Related to the Oceanic Circulation along the South American Continental Margin in the Southwest Atlantic* In: The South Atlantic in the Late Quaternary, Wefer, G., Mulitza, S., Ratmeyer. V., Springer-Verlag, Berlin, Heidelberg, New York, Tokyo, v.(eds), pp. 347–373.

Frenz, M., & Henrich, R. (2007). Carbonate dissolution revealed by silt grain-size distribution: comparison of Holocene and Last Glacial Maximum sediments from the pelagic South Atlantic. *Sedimentology*, 54, 391–404.

Frozza, C.F., Pivel, M.A.G., Suárez-Ibarra, J.Y., Ritter, M.N., & Coimbra, J.C. (2020). Bioerosion on late Quaternary planktonic Foraminifera related to paleoproductivity in the western South Atlantic. *Paleoceanography and Paleoclimatology*, e2020PA003865. https://doi.org/10.1029/2020pa003865

Gonzalez-Silvera, A., Santamaría-del-Angel, E., & Millán-Núñez, R. (2006). Spatial and temporal variability of the Brazil-Malvinas Confluence and the La Plata Plume as seen by SeaWIFS and AVHRR imagery. *Journal of Geophysical Research*, 111: C06010. https://doi.org/10.1029/2004JC002745

Gooday. A.J. (2002). Biological responses to seasonally varying fluxes of organic matter to the ocean floor: A review. *Journal of oceanography*, 58, 305–332. https://doi.org/10.1023/A:1015865826379

Gooday, A.J. (2003). Benthic foraminifera (protista) as tools in deepwater palaeoceanography: environmental influences on faunal characteristics. *Advances in Marine Biology*, 46, 1–90. https://doi.org/10.1016/S0065-28810(03)46002-1

Gordon, A.L., & Greengrove, C.L. (1986). Geostrophic circulation of the Brazil-Falkland confluence. *Deep-Sea Research*, 33(5), 573–585.

Gu, F., Zonneveld, K.A., Chiessi, C.M., Arz, H.W., Pätzold, J., & Behling, H. (2017). Long-term vegetation, climate and ocean dynamics inferred from a 73,500 years old marine sediment core (GeoB2107-3) off southern Brazil. *Quaternary Science Reviews*, 172, 55–71. https://doi.org/10.1016/j.quascirev.2017.06.028

Hales, B. (2003). Respiration, dissolution and the lysocline. *Paleoceanography*, 18(4), 1–14. https://doi.org/10.1029/2003PA000915

Hammer, Øyvind, Harper, David A.T., & Paul D. (2001). Past: Paleontological Statistics Software Package for Education and Data Analysis. *Palaeontologia Electronica*, 4(1), 1–9. http://palaeo-electronica.org/2001_1/past/issue1$_0$1.*htm*

Heil, G.M.N. (2006). *Abrupt Climate Shifts in the Western Tropical to Subtropical Atlantic Region during the Last Glacial.* PhD thesis. Universtity of Bremen, 121.

Hemleben, C., Spindler, M., & Anderson, O.R. (1989). *Modern planktonic foraminifera.* New York, Estados Unidos de América: Springer.

Herguera, J.C. (2000). Last glacial paleoproductivity patterns in the eastern equatorial Pacific: benthic foraminifera records. *Marine Micropaleontology*, 40(3), 259–275. https://doi.org/10.1016/S0377-8398(00)00041-4

Hesse, T., Wolf-Gladrow, D., Lohmann, G., Bijma, J., Mackensen, A., & Zeebe, R.E. (2014). Modelling δ^{13}C in benthic foraminifera: Insights from model sensitivity experiments. *Marine Micropaleontology*, 112, 50–61. https://doi.org/10.1016/j.marmicro.2014.08.001

Hogg, N.G., Owens, W.B., Siedler, G., & Zenk, W. (1996). *Circulation in the deep Brazil Basin*, in Wefer, G., Berger, W.H., Siedler, G., Webb, D.J., eds., The South Atlantic: Present and Past Circulation: Berlin Heidelberg, Springer-Verlag, pp. 13–44

Howe, J.N.W., Piotrowski, A.M., Noble, T.L., Mulitza, S., Chiessi, C.M., & Bayon, G. (2016a). North Atlantic Deep-Water Production during the Last Glacial Maximum. *Nature Communications*. 7, 11765, https://doi.org/10.1038/ncomms11765

Howe, J.N.W., Piotrowski, A.M., Oppo, D.W., Huang, K.F., Mulitza, S., Chiessi, C.M., & Blusztajn, J. (2016b). Antarctic intermediate water circulation in the South Atlantic over the past 25,000 years. *Paleoceanography*, 31, 1302-1314. https://doi.org:10.1002/2016PA002975

Howe, J.N.W., Huang, K.F., Oppo, D.W., Chiessi, C.M., Mulitza, S., Blusztajn, J., Piotrowski, A.M. (2018). Similar mid-depth Atlantic water mass provenance during the Last Glacial Maximum and Heinrich Stadial 1. *Earth and Planetary Science Letters*, 490, 51-61. https://doi.org/10.1016/j.epsl.2018.03.006

Hutson, W.H. (1980). The Agulhas Current During the Late Pleistocene: Analysis of Modern Faunal Analogs. *Science*, 207, 64–66.

Jahnke, R.A., Craven, D.B., McCorkle, D.C., & Reimers, C.E. (1997). $CaCO_3$ dissolution in California continental margin sediments: The influence of orgnic matter remineralization. *Geochimica et Cosmochimica Acta*, 61(17), 3587–3604. https://doi.org/10.1016/S0016-7037(97)00184-1

Jouzel, J., Masson-Delmotte, V., Cattani, O., Dreyfus, G., Falourd, S., Hoffmann, G., Minster, B., Nouet, J., Barnola, J.M., Chappellaz, J., Fischer, H., Gallet, J.C., Johnsen, S., Leuenberger, M., Loulergue, L., Luethi, D., Oerter, H., Parrenin, F., ... Wolff, E.W. (2007). Orbital and Millennial Antarctic Climate Variability over the Past 800,000 Years. *Science*, 317, 793–796. https://doi.org/10.1126/science.1141038

Jöst, A.B., Yasuhara, M., Okahashi, H., Ostmann, A., Martínez-Arbizu, P., & Brix, S. (2017). Vertical distribution of living ostracods in deep-sea sediments, North Atlantic Ocean. *Deep-Sea Research I*, 122, 113-121. https://doi.org/10.1016/j.dsr.2017.01.012

Kemle-von Mücke, S., & Hemleben, C. (1999). *Foraminifera*. In: South Atlantic Zooplankton. Boltovskoy D (ed) Backhuys Publishers, Leiden, pp. 43–73.

Kowsmann, R.O., Lima, A.C., & Vicalvi, M.A. (2014). *Feições indicadoras de instabilidade geológica no talude continental e no Platô de São Paulo*. In: Kowsmann, R.O. (Ed.), Geologia e Geomorfologia. Elsevier, Rio de Janeiro, pp. 71–98. https://doi.org/10.1016/B978-85-352-6937-6.50012-4

Kučera, M. *Planktonic Foraminifera as tracers of past oceanic environments*. In: Hillaire-Marcel, C., de Vernal, A., Chamley, H., editors. Proxies in late cenozoic paleoceanography. vol. 1 of Developments in Marine Geology. Amsterdam: Elsevier; (2007). pp. 213–262.

Lantzsch, H., Hanebuth, T.J.J., Chiessi, C.M., Schwenk, T., & Violante, R.A. (2014). The high-supply, current-dominated continental margin of southeastern South America during the late Quaternary. *Quaternary Research*, 81(2), 339–354. https://doi.org/10.1016/j.yqres.2014.01.003

Laskar, J., Robutel, P., Joutel, F., Gastineau, M., Correia, A., & Levrard, B. (2004). A long-term numerical solution for the insolation quantities of the Earth. *Astronomy & Astrophysics*, 428(1), 261–285. https://doi.org/10.1051/0004-6361:20041335

Le, J., & Shackleton, N.J. (1992). Carbonate dissolution fluctuations in the western equatorial Pacific during the late Quaternary. *Paleoceanography*, 7, 21–42. https://doi.org/10.1029/91PA02854

Lessa, D.V.O., Ramos, R.P., Barbosa, C.F., Da Silva, A.R., Belem, A., Turcq, B., & Albuquerque, A.L. (2014). Planktonic foraminifera in the sediment of a western boundary upwelling system off Cabo Frio, Brazil. *Marine Micropaleontology*, 106, 55–68. https://doi.org/10.1016/j.marmicro.2013.12.003

Lessa, D.V.O., Venancio, I.M., Santos, T.P., Belem, A.L., Turcq, B.J., Sifeddine, A., & Albuquerque, A.L.S. (2016). Holocene oscillations of Southwest Atlantic shelf circulation based on planktonic Foraminifera from an upwelling system (off Cabo Frio, Southeastern Brazil). *The Holocene*, 26(8), 1175–1187. https://doi.org/10.1177/0959683616638433

Lessa, D.V.O., Santos, T.P., Venancio, I.M., & Albuquerque, A.L.S. (2017). Offshore expansion of the Brazilian coastal upwelling zones during Marine Isotope Stage 5. *Global and Planetary Change*, 158, 13-20. https://doi.org/10.1016/j.gloplacha.2017.09.006

Lessa, D.V.O. Santos, T.P., Venancio, I.M., Santarosa, A.C.A., Junior, E.C.S., Toledo, F.A.L., Costa, K.B., & Albuquerque, A.L.S. (2019). Eccentricity-induced expansions of Brazilian coastal upwelling zones. *Global and Planetary Change*, 179, 33-42. https://doi.org/10.1016/j.gloplacha.2019.05.002

Lippold, J., Gruetzner, J., Winter, D., Lahaye, Y., Mangini, A., & Christl, M. (2009). Does sedimentary $^{231}Pa/^{230}Th$ from the Bermuda Rise monitor past Atlantic meridional overturning circulation? *Geophysical Research Letters*, 36, L12601. https://doi.org/10.1029/2009GL038068

Locarnini, R.A., Mishonov, A.V., Antonov, J.I., Boyer, T.P., Garcia, H.E., Baranova, O.K., Zweng, M.M., Paver, C.R., Reagan, J.R., Johnson, D.R., Hamilton, M., & Seidov, D. (2013). *World Ocean Atlas 2013*, Volume 1: Temperature. S. Levitus, Ed., A. Mishonov Technical Ed.; NOAA Atlas NESDIS 73, 40 pp.

Lorius, C., Jouzel, J., Raynaud, D., Hansen, J., & Le Treut, H. (1990). The ice-core record: Climate sensitivity and future greenhouse warming. *Nature*, 347, 139–145. https://doi.org/10.1038/347139a0

Loubere, P. (1991). Deep-sea benthic foraminiferal assemblage response to a surface ocean productivity gradient: a test. *Paleoceanography*, 6, 193–204. https://doi.org/10.1029/90PA02612

Lund, D. C., Tessin, A. C., Hoffman, J. L., & Schmittner, A. (2015). Southwest Atlantic water mass evolution during the last deglaciation. *Paleoceanography*, 30(5), 477–494. https://doi.org/10.1002/2014pa002657

Luz, L.G. Santos, T.P., Eglinton, T.I., Montluçon, D., Ausin, B., Haghipour, N., Sousa, S.M., Nagai, R.H., & Carreira, R.S. (2020). Contrasting late-glacial paleoceanographic evolution between the upper and lower continental slope of the western South Atlantic. *Climate of the Past*, 16, 1245–1261. https://doi.org/10.5194/cp-16-1245-2020

Lynch-Stieglitz, J., Curry, W.B., Oppo, D.W., Ninneman, U.S., Charles, C.D., & Munson, J. (2006), Meridional overturning circulation in the South Atlantic at the last glacial maximum. *Geochemical, Geophysical, Geosystems*, 7, Q10N03. https://doi.org/10.1029/2005GC001226.

Mackensen, A. (2008). *On the use of benthic foraminiferal $\delta^{13}C$ in paleoceanography: constraints from primary proxy relationships.* Geological Society, London, Special Publications, 303, 121–133. https://doi.org/10.1144/SP303.9

Mahiques, M.M., Fukumoto, M.M., Silveira, I.C.A., Figueira, R.C.L., Bícego, M.C., Lourenço, R.A., & Mello-e-Sousa, S.H. (2007). Sedimentary changes on the Southeastern Brazilian upper slope during the last 35,000 years. *Anais da Academia Brasileira de Ciências*, 79(1), 171–181. https://doi.org/10.1590/S0001-37652007000100018

McManus, J.F., Francois, R., Gherardi, J.M., Keigwin, L.D., & Brown-Leger, S. (2004). Collapse and rapid resumption of Atlantic meridional circulation linked to deglacial climate changes. *Nature*, 428(6985), 834–837. https://doi.org/10.1038/nature02494

Milliman, J.D., Troy, P.J., Balch, W.M., Adams, A.K., Li, Y.-H., & Mackenzie, F.T. (1999). Biologically mediated dissolution of calcium carbonate above the chemical lysocline?. *Deep Sea Research Part I: Oceanographic Research Papers*, 46(10), 1653–1669. https://doi.org/10.1016/s0967-0637(99)00034-5

Morard, R., Füllberg, A., Brummer, G.J.A., Greco, M., Jonkers, L., Wizemann, A., Weiner, A.K.M., Darling, K., Siccha, M., Ledevin, R., Kitazato, H., Garidel-Thoron, T., de Vargas, C., & Kučera, M. (2019). Genetic and morphological divergence in the warm-water planktonic foraminifera genus *Globigerinoides*. *PloS One*, 14(12), 1–30. https://doi.org/10.1371/journal.pone.0225246

Nagai, R.H., Ferreira, P.A.L., Mulkherjee, S., Martins, M.V., Figueira, R.C.L., Sousa, S.H.M., & Mahiques, M.M. (2014). Hydrodynamic controls on the distribution of surface sediments from the southeaast South American continental shelf between 23°S and 38°S. *Continental Shelf Research*, 89, 51–60. https://doi.org/10.1016/j.csr.2013.09.016

Naik, S.S., Godad, S.P., Naidu, P.D., Tiwari, M., & Paropkari, A.L. (2014). Early- to late-Holocene contrast in productivity, OMZ intensity and calcite dissolution in the eastern Arabian Sea. *The Holocene*, 26(6), 749–755. https://doi.org/10.1177/0959683614526936

Nees, S., Armand, L., De Deckker, P., Labracherie, M., & Passlow, V. (1999). A diatom and benthic foraminiferal record from the South Tasman Rise (southeastern Indian Ocean): implications for palaeoceanographic changes for the last 200,000 years. *Marine Micropaleontology*, 38(1), 69–89. https://doi.org/10.1016/S0377-8398(99)00039-0

Olsen, A., Key, R.M., van Heuven, S., Lauvset, S.K., Velo, A., Lin, X., Schirnick, C, Kozyr, A, Tanhua, T., Hoppema, M., Jutterström, S., Steinfeldt, R., Jeansson, E., Ishii, M., Pérez, F.F., & Suzuki. T. (2016). The Global Ocean Data Analysis Project version 2 (GLODAPv2) – an internally consistent data product for the world ocean, *Earth System Science Data*, 8(2), 297–323. https://doi.org/10.5194/essd-8-297-2016

Olsen, A., Lange, N., Key, R.M., Tanhua, T., Álvarez, M., Becker, S., Bittig, H.C., Carter, B.R., Cotrim da Cunha, L., Feely, R.A., van Heuven, S., Hoppema, M., Ishii, M., Jeansson, E., Jones, S.D., Jutterström, S., Karlsen, M.K., Kozyr, A., Lauvset, S.K., Lo Monaco, C., Murata, A., Pérez, F.F., Pfeil, B., Schirnick, C., Steinfeldt, R., Suzuki, T., Telszewski, M., Tilbrook, B., Velo, A., & Wanninkhof, R. (2019). GLODAPv2.2019 – an update of GLODAPv2, *Earth System Science Data*. 11, 1437–1461. https://doi.org/10.5194/essd-2019-66

Pereira, L.S., Arz, H.W., Pätzold, J., & Portilho-Ramos, R.C. (2018). Productivity evolution in the South Brazilian Bight during the last 40,000 years. *Paleoceanography and Paleoclimatology*, 33, 1339–1356. https://doi.org/10.1029/2018pa003406

Peterson, R., & Stramma, L. (1991). Upper-level circulation in the South Atlantic Ocean. *Progress in Oceanography*, 26(1), 1–73. https://doi.org/10.1016/0079-6611(91)90006-8

Petit, J.R., Jouzel, J., Raynaud, D., Barkov, N.I., Barnola, J.M., Basile, I., Bender, M., Chappellaz, J., Davis, M., Delaygue, G., Delmotte, M., Kotlyakov, V.M., Legrand, M., Lipenkov, V.Y., Lorius, C., Pépin, L., Ritz, C., Saltzman, E., & Stievenard, M. (1999). Climate and Atmospheric History of the Past 420,000 Years from the Vostok Ice Core, Antarctica. *Nature*, 399, 429–436. https://doi.org/10.1038/20859

Pimenta, F.M., Campos, E.J.D., Miller, J.L., & Piola, A.R. (2005). A numerical study of the Plata River Plume along the Southeastern South American Continental Shelf. *Brazilian Journal of oceanography*, 53(3/4), 129–146. https://doi.org/10.1590/S1679-87592005000200004

Piola, A. R., Campos, E. J. D., Möller, O. O., Charo, M., & Martinez, C. (2000). Subtropical Shelf Front off eastern South America. *Journal of Geophysical Research*, 105(C3), 6565–6578.

Piola, A.R., Matano, R.P. *Ocean Currents: Atlantic Western Boundary—Brazil Current/Falkland (Malvinas) Current*, in Encyclopedia of Ocean Sciences, (2017), pp. 422–430. https://doi.org/10.1016/B978-0-12-409548-9.10541-X

Piola, A.R., Matano, R.P., Palma, E.D., Möller, O.O., Campos, & E.J.D. (2005). The influence of the Plata River discharge on the western South Atlantic shelf. *Geophysical Research Letters*, 32(1), (L01603). https://doi.org/10.1029/2004GL021638

Portilho-Ramos, R.C., Ferreira, F., Calado, L., Frontalini, F., & de Toledo, M.B. (2015). Variability of the upwelling system in the southeastern Brazilian margin for the last 110,000 years. *Global and Planetary Change*, 135, 179–189. https://doi.org/10.1016/j.gloplacha.2015.11.003

Portilho-Ramos, R.C., Pinho, T.M.L., Chiessi, C.M., & Barbosa, C.F. (2019). Understanding the mechanisms behind high glacial productivity in the southern Brazilian margin. *Climate of the Past*, 15(3), 943–955. https://doi.org/10.5194/cp-15-943-2019

Prell, W.L., & Curry, W.B. (1981). Faunal and isotopic indices of monsoonal upwelling: Western Arabian Sea. *Oceanologica acta*, 4(1), 91–98.

R Core Team. (2019). *R: a language and environment for statistical computing.* Vienna, Austria: R Foundation for Statistical Computing. http://www.R-project.org/

Rasmussen, T.L., Thomsen, E., Troelstra, S.R., Kuijpers, A., & Prins, M.A. (2002). Millennial-scale glacial variability versus Holocene stability: changes in planktic and benthic foraminifera faunas and ocean circulation in the North Atlantic during the last 60,000 years. *Marine Micropaleontology*, 47(1–2), 143–176. https://doi.org/10.1016/S0377-8398(02)00115-9

Ravello, A.C., & Hillaire-Marcel, C. (2007). *The use of oxygen and carbon isotopes of foraminifera in paleoceanography.* In: Proxies in late Cenozoic Paleoceanography. Hillaire-Marcel, C., De Vernal, A. (Eds.). Developments in Marine Geology, Elsevier, Amsterdam, 843 pp.

Reid, J.L., Nowlin Jr., W.D., & Patzert, W.C. (1976). On the characteristics and circulation of the Southwestern Atlanitc Ocean. *Journal of physical oceanography*, 7, 62–91. https://doi.org/10.1175/1520-0485(1977)007¡0062:OTCACO¿2.0.CO;2

Rex, M.A., Etter, R.J., Morris, J.S., Crouse, J., McClain, C.R., Johnson, N.A., Stuart, C.T., Deming, J.W., Thies, R., & Avery, R. (2006). Global bathymetric patterns of standing stock and body size in the deep-sea benthos. *Marine Ecology Progress Series*, 317, 1–8. https://doi.org/10.3354/meps317001.

Rex, M.A., & Etter, R.J. (2010). *Deep-sea biodiversity: pattern and scale.* Harvard University Press, Cambridge, pp. 354.

Santos, T.P., Lessa, D.O., Venancio, I.M., Chiessi, C.M., Mulitza, S., Kuhnertb, H., Govind, A., Machado, T., Costa, K.B., Toledo, F., Dias, B.B., & Albuquerque, A.L.S. (2017). Prolonged warming of the Brazil Current precedes deglaciations. *Earth and Planetary Science Letters*, 463, 1–12. https://doi.org/10.1016/j.epsl.2017.01.014

Savian, J.F., Pivel, M.A.G., Frigo, E., Rocha, J.A., Lopes, C.T., Suárez-Ibarra, J.Y., Coimbra, J.C., Petró, S.M., Leonhardt, A., Callefo, F., Hartmann, G.A., Braga, A.H., Trindade, R.I.F., Rodelli, D., Jovane, L., Environmental magnetic record of sediments from the western South Atlantic since Marine Isotope Stage 3. Paper submitted to *Global & Planetary Change*.

Schiebel, R. (2002). Planktic foraminiferal sedimentation and the marine calcite budget. *Global Biogeochemical Cycles*, 16(4), 1–21. https://doi.org/10.1029/2001GB001459

Schiebel, R., & Hemleben, C. (2017). *Planktic Foraminifers in the Modern Ocean*, pp. 358. Berlin, Germany: Springer. https://doi.org/10.1007/978-3-662-50297-6

Schlitzer, R. (2020). Ocean data view. Available from: https://odv.awi.de

Schmiedl, G., Pfeilsticker, M., Hemleben, C., & Mackensen, A. (2004). Environmental and biological effects on the stable isotope composition of recent deep-sea benthic foraminifera from the western Mediterranean Sea. *Marine Micropaleontology*, 51, 129-152. https://doi:10.1016/j.marmicro.2003.10.001

Shackleton, N.J. (2000). The 100,000-year ice-age cycle identified and found to lag temperature, carbon dioxide, and orbital eccentricity. *Science*, 289, 1897–1902. https://doi.org/10.1126/science.289.5486.1897

Shakun, J.D., Clark, P.U., He, F., Marcott, S.A., Mix, A.C., Liu, Z., Otto-Bliesner, B., Schmittner, A., & Bard, E. (2012). Global warming preceded by increasing carbon dioxide concentrations during the last deglaciation. *Nature*, 484, 49–55. https://doi.org/10.1038/nature10915

Siccha, M., & Kučera, M. (2017). ForCenS, a curated database of planktonic foraminifera census counts in marine surface sediment samples. *Scientific Data*, 4, 170109. https://doi.org/10.1038/sdata.2017.109

Silveira, I.C.A., Schmidt, A.C.K., Campos, E.J.D., Godoi, S.S., & Ikeda, Y. (2000). A corrente do Brasil ao Largo da Costa Leste Brasileira. *Revista Brasileira de Oceanografia*, 48(2), 171–183. https://doi.org/10.1590/S1413-77392000000200008

Smith, C.R., Berelson, W., Demaster, D.J., Dobbs, F.C., Hammond, D., Hoover, D.J., Pope, R.H., & Stephens, M. (1997). Latitudinal variations in benthic processes in the abyssal equatorial Pacific: control by biogenic particle flux. *Deep Sea Research Part II: Topical Studies in Oceanography*, 44(9–10), 2295–2317. https://doi.org/10.1016/S0967-0645(97)00022-2

Sousa, S.H.M., de Godoi, S.S., Amaral, P.G.C., Vicente, T.M., Martins, M.V.A., Sorano, M.R.G.S., Gaeta, S.A., Passos, R.F., & Mahiques, M.M. (2014). Distribution of living planktonic foraminifera in relation to oceanic processes on the southeastern continental Brazilian margin (23°S–25°S and 40°W–44°W). *Continental Shelf Research*, 89, 76–87. https://doi.org/10.1016/j.csr.2013.11.027

Souto, D.D., Lessa, D.V.O., Albuquerque, A.L.S., Sifeddine, A., Turcq, B.J., & Barbosa, C.F. (2011). Marine sediments from southeastern Brazilian continental shelf: A 1200 year record of upwelling productivity. *Palaeogeography, palaeoclimatology, palaeoecology*, 299, 49–55. https://doi.org/10.1016/j.palaeo.2010.10.032

Suárez-Ibarra, J.Y., Frozza, C.F., Petró, S.M., & Pivel, M.A.G. (accepted). Fragment or broken? Improving the planktonic Foraminifera fragmentation assessment. *PALAIOS*

Stramma, L., & England, M. (1999). On the water masses and mean circulation of the South Atlantic Ocean. *Journal of Geophysical Research*, 104(C9), 20863–20883. https://doi.org/10.1029/1999JC900139

Toledo, F.A.L., Cachão, M., Costa, K.B., & Pivel, M.A.G. (2007). Planktonic foraminifera, calcareous nannoplankton and ascidian variations during the last 25 kyr in the South-western Atlantic: A paleoproductivity signature?. *Marine Micropaleontology*, 64(1–2), 67–79. https://doi.org/10.1016/j.marmicro.2007.03.001

Toledo, F.A.L., Costa, K.B., Pivel, M.A.G., & Campos, E.J.D. (2008). Tracing past circulation changes in the western South Atlantic based on planktonic Foraminifera. *Revista brasileira de paleontologia*, 11(3), 169–178. https://doi.org/10.4072/rbp.2008.3.03

Venancio, I.M., Belem, A.L., Santos, T.H., Zucchi, M., Azevedo, A.E., Capilla, R., & Albuquerque, A.L.S. (2014). Influence of continental shelf processes in the water mass balance and productivity from stable isotope data on the Southeastern Brazilian coast. *Journal of Marine Systems*, 139, 241–247. https://doi.org/10.1016/j.jmarsys.2014.06.009

Venancio, I.M., Gomes, V.P., Belem, A.L., & Albuquerque, A.L.S. (2016). Surface-to-subsurface temperature variations during the last century in a western boundary upwelling system (Southeastern, Brazil). *Continental Shelf Research*, 125, 97–106. https://doi.org/10.1016/j.csr.2016.07.003

Villanueva, J., Grimalt, J.O., Labeyrie, L.D., Cortijo, E., Vidal, L., & Louis-Turon, J. (1998). Precessional forcing of productivity in the North Atlantic Ocean. *Paleoceanography*, 13(6), 561–571. https://doi.org/10.1029/98PA02318

Waelbroeck, C., Labeyrie, L., Michel, E., Duplessy, J.C., McManus, J., Lambeck, K., Balbon, E., & Labracherie, M. (2002). Sea-level and deep-water temperature changes derived from benthic Foraminifera isotopic records. *Quaternary Science Reviews*, 21, 295–305. https://doi.org/10.1016/S0277-3791(01)00101-9

Weschenfelder, J., Baitelli, R., Corrêa, I.C.S., Bortolin, E.C., & dos Santos, C.B. (2014). Quaternary incised valleys in southern Brazil coastal zone. *Journal of South American Earth Sciences*, 55, 83–93. https://doi.org/10.1016/j.jsames.2014.07.004

Wefer, G., Berger, W.H., Bijma, J., & Fischer, G. (1999). *Clues to ocean history: A brief overview of proxies.* In: Fischer, G.; Wefer, G., (Eds.) Use of Proxies in Paleoceanography: Examples from the South Atlantic. Springer-Verlag, Berlin Heidelberg, pp. 68.

Yasuhara, M., Hunt, G., Cronin, T.M., Hokanishi, N., Kawahata, H., Tsujimoto, A., & Ishitake, M. (2012). Climatic forcing of Quaternary deep-sea benthic communities in the North Pacific Ocean. *Paleobiology*, 38(1), 162–179. https://doi.org/10.1666/10068.1

Zamelczyk, K., Rasmussen, T.L., Husum, K., Haflidason, H., de Vernal, A., Ravna, E.K., Hald, M., & Hillaire-Marcel, C. (2012). Paleoceanographic changes and calcium carbonate dissolution in the central Fram Strait during the last 20 ka. *Quaternary Research*, 78, 405–416. https://doi.org/10.1016/j.yqres.2012.07.006

Zweng, M.M, Reagan, J.R., Antonov, J.I., Locarnini, R.A., Mishonov, A.V., Boyer, T.P., Garcia, H.E., Baranova, O.K., Johnson, D.R., Seidov, D., & Biddle, M.M. (2013). *World Ocean Atlas 2013*, Volume 2: Salinity. S. Levitus, Ed., A. Mishonov Technical Ed.; NOAA Atlas NESDIS 74, 39 pp.

Paleoceanography and Paleoclimatology

Supporting Information for

Calcium carbonate dissolution triggered by high productivity during the last glacial-interglacial interval at the deep western South Atlantic

J.Y. SUAREZ-IBARRA[1,2], C.F. FROZZA[1], S.M. PETRÓ[3], P.L. PALHANO[1], M.A.G. PIVEL[4]

[1]Programa de Pós-Graduacão em Geociências, Instituto de Geociências, Universidade Federal do Rio Grande do Sul, Av. Bento Gonçalves, 9500, Cx. P. 15001, 91501-970, Porto Alegre, RS, Brazil.
[2]Ústav Geologie a Paleontologie, Přírodovědecká fakulta, Univerzita Karlova, Albertov 6, Praha 2, 12843, Czech Republic, present address.
[3]ITT FOSSIL - Instituto Tecnológico de Micropaleontologia, Universidade do Vale do Rio dos Sinos, Av. UNISINOS, 950, 93022-750, São Leopoldo, RS, Brazil.
[4]Instituto de Geociências, Universidade Federal do Rio Grande do Sul, Av. Bento Gonçalves, 9500, Cx. P. 15001, 91501-970, Porto Alegre, RS, Brazil.

Contents of this file

Table S1
Figure S1
Text S1
Figure S2
Tables S2 and S3
Appendix S1

Introduction

The present Supporting Information file presents data for: i) other analyzed cores (Table S1), ii) the Sea Surface Temperature (SST) residuals (Figure S1), iii) the age model construction (Figure S1, Table S2 and Table S3), as well as iv) the appendix of planktonic Foraminifera species (Appendix S1).

Table S1

In the manuscript Figure 1 are shown the core SAT-048A location, as well as the location of the other analyzed cores. Names, coordinates, and depths below sea level of the mentioned cores are shown in Table S1.

Table S1. Location of the other analyzed cores, all recovered from the western South Atlantic.

Core	Lat	Long	Depth (mbsl)
SAN-76	24°25'S	42°16'W	1682
GL-852	25°0'S	43°33'W	1938
GeoB2107-3	27°10'S	46°27'W	1048
GeoB2104-3	27.3°S	46.4°W	1500
JPC-17	27°41'S	46°29'W	1627
SAT-048A	29°11'S	47°15'W	1542
SIS-188	29°22'S	47°28'W	1514

Figure S1

The SST estimates at 100 m waters below sea level, performed on the present study, are show in manuscript Figure 4. Residual of this reconstruction is showed in Figure S1. The 95% of the residuals are located between 2.5 and -2.5°C, while the 90% are between 1.8 and -1.8°C.

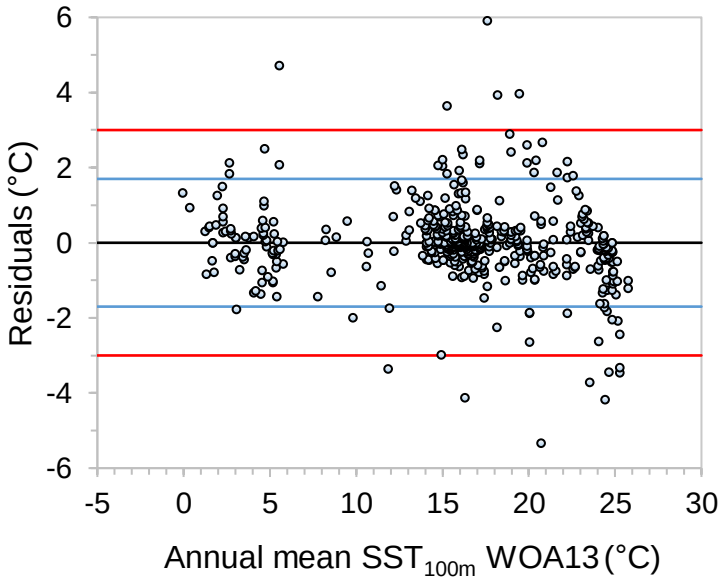


Figure S1. Residuals vs. Annual mean SST estimates at 100 m waters below sea level for core SAT048A. Red lines encompass 95% of the residuals (between 2.5 and -2.5°C) and blue lines encompass 90% (between 1.8 and -1.8°C).

Text S1.

From the 54 samples, a total of 21,962 specimens of planktonic Foraminifera were classified into 28 morphospecies (supplemental material). A total of 4878 specimens of benthic Foraminifera were counted. Table S1 lists the morphospecies, total relative abundance and total absolute abundance in descending order. The dominant species in the associations were *Globigerinoides ruber albus*, with a maximum relative abundance of 25.32%, followed by *Globigerinita glutinata* (15.56%) and *Globigerina bulloides* (15.56%). Other representative but less abundant species are *Neogloboquadrina incompta* (8.57%), *Globigerinoides ruber ruber* (8.22%) and *Globoconella inflata* (7.69%).

Other species, with total relative abundances between 5 and 1% are (in decreasing order): *Trilobatus trilobus*, *Globoturborotalita tenellus, Neogloboquadrina dutertrei, Globorotalia scitula, Globoturborotalita rubescens, Globigerinella calida, Globorotalia truncatulinoides* (R)*, Globorotalia crassaformis* and *Globorotalia truncatulinoides* (L).

Finally, species with extremely low total absolute abundance (> 1%) are *Candeina nitida, Globigerina falconensis, Globigerinella siphonifera, Globigerinoides conglobatus, Globorotalia hirsuta, Globorotalia menardii*, *Globorotalia tumida, Neogloboquadrina pachyderma, Orbulina universa, Pulleniatina obliquiloculata, Trilobatus sacculifer, Turborotalita humilis* and *Turborotalita quinqueloba.*

Age Model

The performing results of the rBacon package for core SAT-048A are shown in Figure S2. It is possible to see the ^{14}C correlation points, as wells as the identified Laschamp geomagnetic excursion (Savian et al., submitted).

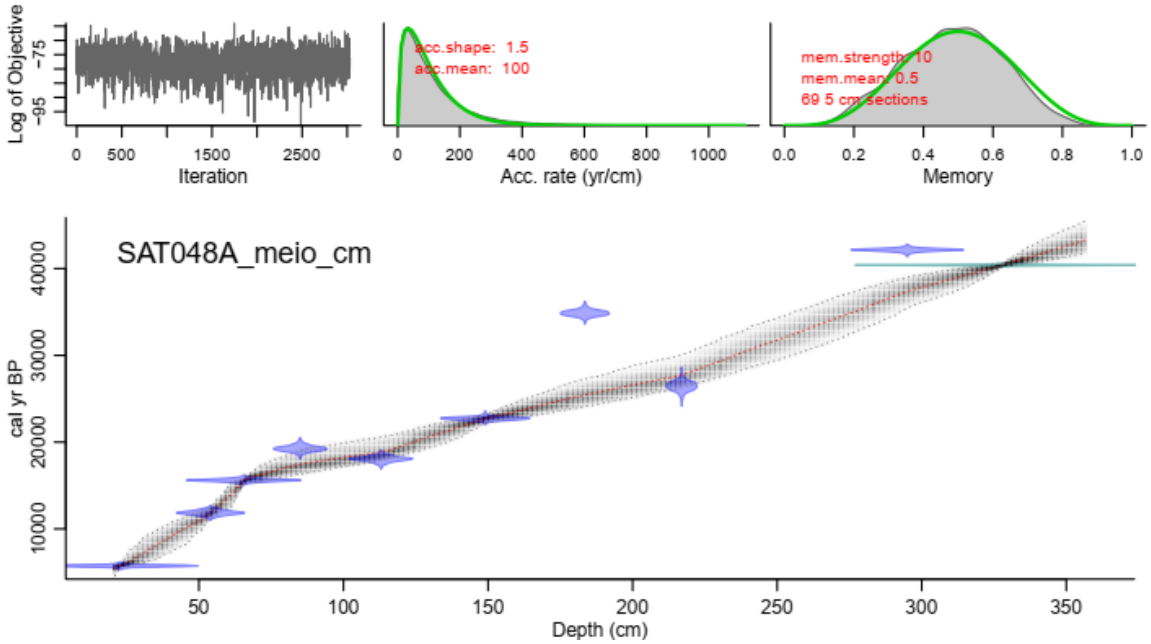


Figure S2. Age-depth plot for core SAT048A (bottom panel). The red stippled line indicates the mean age-depth model, 95% confidence ranges indicated by dark-grey stippled curves and calibrated dates in blue. Upper panels from left to right display (1) the Markov chain Monte Carlo (MCMC) iterations, the prior (green curves) and posterior (grey histograms) distributions for (2) the sedimentation rate and (3) memory.

The AMS ^{14}C results of core SAT-048A (Frozza et al., 2020) are shown in Table S2. The Marine Reservoir Correction Database (Delta R= -85 +/-40) is based on ages from Nadal de Masi (1999), Angulo et al. (2005), and Alves et al. (2015). Rbacon package (Blaauw & Christen, 2011; version 2.4.2), for open source R software (R Core Team, 2020), used the calibration curve Marine20 (Heaton et al., 2020).

Table S2. SAT-048A (Frozza et al., 2020) AMS ^{14}C ages.

Sample depth (cm)	LAC-UFF sample code	Species	Age ^{14}C (ka BP)	Error (ka)
23	170059	*G. menardii*	5.226	0.028
23	170209	*G. ruber*	5.471	0.032
54	180167	*G. ruber*	10.594	0.117
65	190321	*G. ruber*	13.548	0.038
85	180168	*G. ruber*	16.599	0.212
113	180169	*G. ruber*	15.531	0.185
149	190704	*G. ruber*	19.536	0.104
183.5	190323	*G. ruber*	31.174	0.271
217	180170	*G. ruber*	22.997	0.451
295	190540	*G. ruber*	38.997	0.260

Table S2 shows data the radiocarbon data published by Frozza et al., 2020 used for the former age model.

Table S3. SAT-048A data points for age model building on rbacon package.

LabID	Age	Error	Depth_cm	cc	delta.R	delta.STD
LACUFF170059	5226	28	23	2	-85	40
LACUFF170209	5471	32	23	2	-85	40
LACUFF180167	10594	117	54	2	-85	40
LACUFF190321	13548	38	65.5	2	-85	40
LACUFF180168	16599	212	85	2	-85	40
LACUFF180169	15531	185	113	2	-85	40
LACUFF190704	19536	104	149	2	-85	40
LACUFF190323	31174	271	183.5	2	-85	40
LACUFF180170	22997	451	217	2	-85	40
LACUFF190540	38997	260	295	2	-85	40
Laschamp	41000	0	328	0	0	0

Table S3 shows data used for the age model (Figure S2) building. Laschamp (Table S3) correlation point is from Savian et al. (submitted).

Appendix S1. List of the species/morphospecies/subspecies identified and their total relative and absolute abundances.

Species/ Morphospecies/subspecies	Total relative abundance (%)	Total absolute abundance
Globigerinoides ruber albus	25.32	5573
Globigerinita glutinata	15.56	3391
Globigerina bulloides	15.56	3355
Neogloboquadrina incompta	8.57	1892
Globigerinoides ruber ruber	8.22	1828
Globoconella inflata	7.69	1701
Trilobatus trilobus	2.22	492
Globoturborotalita tenellus	2.22	480
Neogloboquadrina dutertrei	1.64	371
Globorotalia scitula	1.50	322
Globoturborotalita rubescens	1.46	314
Globigerinella calida	1.29	292
Globorotalia truncatulinoides (R)	1.28	295
Globorotalia crassaformis	1.28	289
Globorotalia truncatulinoides (L)	1.16	258
Triolobatus sacculifer	0.93	212
Globigerina falconensis	0.89	193
Globorotalia hirsuta	0.62	135
Globigerinella siphonifera	0.41	93
Globorotalia menardii	0.37	77
Orbulina universa	0.36	79
Turborotalita quinqueloba	0.32	67
Globigerinoides conglobatus	0.32	70
Neogloboquadrina pachyderma	0.24	54
Pulleniatina obliquiloculata	0.21	44
Globorotalia tumida	0.07	16
Turborotalita humilis	0.04	9
Candeina nitida	0.04	8

References

Alves, E., Macario, K., Souza, R., Pimenta, A., Douka, K., Oliveira, F., Chanca, I., & Ângulo, E. (2015). Radiocarbon reservoir corrections on the Brazilian coast from pre-bomb marine shells. *Quaternary Geochronology*, 29, 30–35. doi:10.1016/j.quageo.2015.05.006

Angulo, R.J., de Souza, M.C., Reimer, P.J., & Sasaoka, S.K. (2005). Reservoir effect of the southern and southeastern Brazilian coast. *Radiocarbon*, 47, 67–73. doi:10.1017/S0033822200052206

Blaauw, M., & Christen, J.A. (2011). Flexible Paleoclimate Age-Depth Models using autoregressive gamma process. *Bayesian Analysis,* 6(3), 457–474. doi:10.1214/11-BA618

Frozza, C.F., Pivel, M.A.G., Suárez-Ibarra, J.Y., Ritter, M.N., &, Coimbra, J.C., 2020. Bioerosion on late Quaternary planktonic Foraminifera related to paleoproductivity in the western South Atlantic. *Paleoceanography and Paleoclimatology*, 35, e2020PA003865. doi:10.1029/2020PA003865

Heaton, T., Köhler, P., Butzin, M., Bard, E., Reimer, R., Austin, W., … Skinner, L. (2020). Marine20—The Marine Radiocarbon Age Calibration Curve (0–55,000 cal BP). *Radiocarbon* 62 (4), 779-820. doi:10.1017/RDC.2020.68

Lisiecki, L.E., & Stern, J.V. (2016). Regional and global benthic $\delta^{18}O$ stacks for the last glacial cycle. *Paleoceanography*, 31 (10), 1368–1394. doi:10.1002/2016PA003002

Nadal De Masi, M. A. (1999). *Prehistoric hunter-gatherer mobility on the southern Brazilian coast: Santa Catarina Island*. Ph.D. Thesis, Stanford University, Palo Alto, CA (unplublished).

R Core Team. (2020). *R: a language and environment for statistical computing*. Vienna, Austria: R Foundation for Statistical Computing. http://www.R-project.org/

Savian, J.F., Pivel, M.A.G., Frigo, E., Rocha, J.A., Lopes, C.T., Suárez-Ibarra, J.Y., Coimbra, J.C., Petró, S.M., Leonhardt, A., Callefo, F., Hartmann, G.A., Braga, A.H., Trindade, R.I.F., Rodelli, D., & Jovane, L. Environmental magnetic record of sediments from the western South Atlantic since Marine Isotope Stage 3. Paper submitted to *Global & Planetary Change*.